Hindawi
Advances in High Energy Physics
Volume 2022, Article ID 7373365, 24 pages
https://doi.org/10.1155/2022/7373365

Research Article

Calculated Event Rates for Axion Detection via Atomic and Nuclear Processes

John D. Vergados,[1,2] **Paraskevi C. Divari**,[3] **and Hiroyasu Ejiri**[4]

[1]*University of Ioannina, Ioannina GR 451 10, Greece*
[2]*Center for Axion and Precision Physics Research, IBS, Daejeon 34051, Republic of Korea*
[3]*Department of Physical Sciences and Applications, Hellenic Military Academy, Vari, 16673 Attica, Greece*
[4]*Research Center for Nuclear Physics, Osaka University, Osaka 567-0047, Japan*

Correspondence should be addressed to Paraskevi C. Divari; pdivari@gmail.com

Received 20 December 2021; Accepted 20 January 2022; Published 22 February 2022

Academic Editor: Luciano Petruzziello

The possibility of detection of 5.5 MeV and 14.4 keV solar axions by observing axion-induced nuclear and atomic transitions is investigated. The presence of nuclear transitions between spin orbit partners can be manifested by the subsequent deexcitation via gamma ray emissions. The transition rates can also be studied in the context of radiative axion absorption by a nucleus. The elementary interaction is obtained in the context of the axion-quark couplings predicted by existing axion models. Then, these couplings will be transformed to the nucleon level utilizing reasonable existing models, which lead to effective transition operators. Using these operators, we calculate the needed nuclear matrix elements employing wave functions obtained in the context of the nuclear shell model. With these ingredients, we discuss possibilities of experimental observation of the axion-induced nuclear gamma rays. In the second part, we will examine the axion-induced production of X-rays (axion-photon conversion) or ionization from deeply bound electron orbits. In this case, the axion electron coupling is predicted by existing axion models; no renormalization is needed. The experimental signal is the observation of directly produced electrons and/or the emission of hard X-rays and Auger electrons, following the deexcitation of the final atom. Critical discussion is made on the experimental feasibility of detecting the solar axions by using multiton scale NaI detectors.

1. Introduction

In the standard model, there is a source of CP violation from the phase in the Kobayashi-Maskawa mixing matrix. This, however, is not large enough to explain the baryon asymmetry observed in nature. Another source is the phase in the interaction between gluons (θ-parameter), naively expected to be of order unity. The nonobservation, however, of elementary electron dipole moment set limits its value to be $\theta \leq 10^{-9}$. This has been known as the strong CP problem. A solution to this problem has been the P-Q (Peccei-Quinn) mechanism. In extensions of the standard model (S-M), e.g. two Higgs doublets, the Lagrangian has a global P-Q chiral symmetry $U_{PQ}(1)$, which is spontaneously broken, generating a Goldstone boson, the axion (a). In fact, the axion has been proposed a long time ago as a solution to the strong CP problem [1] resulting to a pseudo-Goldstone boson [2, 3]. The two most widely cited models of invisible axions are the KSVZ (Kim, Shifman, Vainshtein, and Zakharov) or hadronic axion models [4, 5] and the DFSZ (Dine, Fischler, Srednicki, and Zhitnitskij) or GUT axion model [6, 7]. This also led to the interesting scenario of the axion being a candidate for dark matter in the universe [8–10], and it can be searched for by real experiments [11–14]. For a recent review, see [15]. The relevant phenomenology has also been reviewed [16].

Axions could be generated mainly by bremsstrahlung processes and Compton scattering [17], originally proposed for star cooling via axion emission; see, e.g., [18] and a more recent work [19] for Bremsstrahlung processes and Compton scattering studied a long time ago [20] and more recently [21], also generated via the Primakoff conversion

of photons to axions in the presence of a magnetic field [22]. All these yield a continuous axion spectrum, the Primakoff conversion with an average energy around 4 keV [23]. They can also be generated by nuclear transitions, which involve monochromatic axions, e.g., 14.4 keV in the case of the deexcitation of ^{57}Fe$*$ and 5.5 MeV in the case $p + d \longrightarrow {}^3_2\mathrm{He}*$. Axions produced in nuclear processes are monoenergetic because their energies correspond to the transition energies to specific nuclear states. These solar axions can be emitted and escape from the solar core due to the very weak interaction between the axion and matter.

In the Intensity Frontier of physics, a search for new light particles, including axions among others, is growing. Generally speaking, axions can be produced in an environment of intense photon production. The axion sources considered so far are cosmological or in the sun. Such environment on earth can be the core of a nuclear reactor; see, e.g., the recent works [24, 25]. It is, of course, well-known that neutrinos were first detected in reactors and the most accurate neutrino oscillation parameters were determined using reactor neutrinos. It is amusing to think that history may repeat itself; i.e., reactors may have the potential to produce axion-like particles (ALPs) of sufficient intensity through Primakoff conversion, Compton-like processes, and nuclear transitions as well as dark photons. The ALPs can subsequently interact with the material of a nearby detector via the standard processes, i.e., the inverse Primakoff effect, the inverse Compton-like scatterings, and via axioelectric absorption. It is claimed [24, 25] that reactor-based neutrino experiments have a high potential to test ALP-photon couplings and masses.

Searches for solar axions have been carried out with various experimental techniques: magnetic helioscopes [26, 27], low-temperature bolometers [28], and thin foil nuclear targets [29]. CUORE (Cryogenic Underground Observatory for Rare Events) [30–34] and the Majorana Demonstrator [35] which are designed to search for neutrinoless double beta decay ($0\nu\beta\beta$) using very low background detectors are used for the axion searches. The Ge detectors in GERDA [36] can also be used to search for dark matter weakly interacting massive particles (WIMPs) and axion searches [37–39].

As we have mentioned, high-energy axions can be produced in the sun, e.g., in the kiloelectron volt range, by the deexcitation of ^{57}Fe$*$ [40] or even at the MeV range [41–43] via the following reaction:

$$\begin{aligned} &p + d \longrightarrow {}^3_2\mathrm{He} + a(5.5)\mathrm{MeV} \text{ together with the observed} \\ &p + d \longrightarrow {}^3_2\mathrm{He} + \gamma(5.5)\mathrm{MeV} \end{aligned} \quad (1)$$

Both solar axions mentioned above can be exploited for axion detection. Those in the energy range of Equation (1) are suitable for the study of axion-induced nuclear transitions in the laboratory, while the kiloelectron volt axions for atomic processes. To this end, in Section 2, we will discuss the particle model needed in understanding these processes. In Section 3, we discuss how one obtains a set of axion-nucleon couplings g_{aN}, going from the quark to the nucleon level, needed in constructing the effective nuclear transition operators. In Section 4, we will briefly discus the experimental issues involved in the detection of axions in large detectors involving materials like NaI. In Section 5, we will derive the cross sections needed for the rates: (A) in the case of spin-induced nuclear transitions, (B) the radiative axion absorption by nuclei, and (C) axion-induced weak process induced by axion absorption. Then, in Section 6, we will briefly discuss the nuclear model needed to evaluate the cross sections for cases (A) and (B) above for the Na and I nuclei. In Section 7, we will present the obtained nuclear matrix elements for the nuclei of interest and we will exhibit our results for the relevant cross sections and the obtained event rates.

After that, we will utilize the Fe$*$-57 14.4 keV source, which is ideal to study axion-induced atomic processes. Thus, after determining the axion-electron coupling from the Borexiono experiment in Section 8, we will calculate in Sections 9 and 10 the cross sections for axion-induced atomic transitions and ionization from deeply bound orbits. In this case, one expects good experimental signatures; in addition to observing the primary electrons, one expects signals of hard X-rays and Auger electrons, following the atomic deexcitation.

2. The Particle Model

We remind the reader that the axion, a, is a pseudoscalar particle with a coupling to fermions.

(i) The axion coupling to the electron can be described by a Lagrangian of the form

$$\mathscr{L} = \frac{g_e}{f_a} i\partial_\mu a \bar{\psi}_e\left(\mathbf{p}', s\right)\gamma^\mu\gamma_5\psi_e(\mathbf{p}, s), \quad (2)$$

where g_e is a coupling constant and f_a a scale parameter with the dimension of energy. g_e can be calculated in various axion models. For an axion with mass m_a, it easy to show that in the nonrelativistic limit,

(a) the time component $\mu = 0$ is given by

$$\mathscr{L} = \langle\phi|\Omega|\phi\rangle, \quad \Omega = \frac{g_e m_a}{2f_a}\frac{\boldsymbol{\sigma}.\mathbf{q}}{m_e}, \quad \mathbf{q} = \mathbf{p}' - \mathbf{p}, \quad (3)$$

which is negligible for $m_a << m_e$

(b) the space component, $\mu \neq 0$,

$$\mathscr{L}_{aee} = \langle\phi|\Omega|\phi\rangle, \quad \Omega = \frac{g_e}{2f_a}\boldsymbol{\sigma}.\mathbf{q}, \quad \mathbf{q} = \mathbf{p}' - \mathbf{p}, \quad (4)$$

where p and p' are the initial and final electron momenta, f_a the axion decay constant, and σ the spin of the electron

(ii) the axion coupling to the quarks is similarly given by

$$\mathscr{L} = \frac{g_q}{f_a} i\partial_\mu a \bar{\psi}_q\left(\mathbf{p}', s\right)\gamma^\mu\gamma_5\psi_q(\mathbf{p}, s), \tag{5}$$

where g_q is the coupling constant. The space component, $\mu \neq 0$, in the nonrelativistic limit is given by

$$\mathscr{L}_{aee} = \langle\phi|\Omega|\phi\rangle, \quad \Omega = \frac{g_{aq}}{2f_a}\boldsymbol{\sigma}.\mathbf{q}, \tag{6}$$

with σ the Pauli matrices and ϕ the quark wave function, and q is the axion momentum

We will concentrate on the last term involving the operator $g_{aq}\sigma$. The quantities g_{aq} can be evaluated at various axion models.

$$\mathrm{me}_q = \left\langle q\left|\left(g^0_{aq} + g_{as} + g^3_{aq}\tau_3\right)\sigma\right|q\right\rangle, \tag{7}$$

where we have ignored the contribution of heavier quarks, and thus, the isovector and isoscalar components become

$$g^3_{aq} = \frac{1}{2}(g_{au} - g_{ad}), \quad g^0_{aq} = \frac{1}{2}(g_{au} + g_{ad}). \tag{8}$$

Some authors use the notation c_q instead of g_{aq}.

The scale parameter f_a has been related to the axion mass m_a via the relation

$$\frac{1}{f_a} = \frac{m_a}{\Lambda^2_{\mathrm{QCD}}}, \tag{9}$$

with $\Lambda_{\mathrm{QCD}} = 218\,\mathrm{MeV}$. For the determination of Λ_{QCD}, see Particle Data Group [44]. More recently, however, a model-independent relation has been provided [45].

$$m_a f_a = 5.691(51) \times 10^3 \mathrm{MeV}^2. \tag{10}$$

We will employ the expression

$$m_a f_a \approx 6000\mathrm{MeV}^2. \tag{11}$$

Taking f_a to be $10^{10}\,\mathrm{MeV}$, then $m_a = 0.6\,\mathrm{eV}$.

3. The Effective Axion-Nucleon Couplings

In this section, we follow the procedure discussed in a previous work [40] and references therein. For the benefit of the reader, we are going to give a summary here.

In going from the quark to the nucleon level, one can follow a procedure analogous for the determination of the nucleon spin from that of the quarks [46, 47]. The matrix element at the nucleon level can be written as

$$\mathrm{me}_N = \left\langle N\left|g^0_{aq}(\delta_0 - \Delta s) + g_{as}\Delta s + g^3_{aq}\tau_3\delta_1\right)\sigma\right|N\right\rangle, \tag{12}$$

where

$$\begin{aligned}\delta_0 &= (\Delta u + \Delta d + \Delta s),\\ \delta_1 &= (\Delta u - \Delta d),\end{aligned} \tag{13}$$

$\delta_0 - \Delta s = \Delta u + \Delta d$. The quantities $\Delta u, \Delta d$, and Δs have been obtain previously [40]. Alternatively, these quantities can be expressed in terms of the quantities D and F defined by Ellis [48]

$$\begin{aligned}\delta_1 &= F + D,\\ \delta_0 &= 3F - D + 3\Delta s.\end{aligned} \tag{14}$$

The quantity δ_1 is essentially fixed by the axial current to be approximately 1.27 of the vector current. No such constraint exists for the isoscalar part, so for that, we have to rely on models. For the quantities D and F, one can use experimental information [48]. Thus, e.g., from hyperon beta decays and flavor SU(3) symmetry, one gets

$$\frac{3F - D}{\sqrt{3}} = 0.34 \pm 0.02. \tag{15}$$

Different approaches have been suggested by Kaplan [17], based on the DFSZ [7, 9] axion, which is analyzed in some detail in ref. [40].

On the other hand, measurements of νp and $\nu\bar{p}$ elastic scattering of the recent MicroBooNE experiment [49] indicate that $\Delta s = \pm 0.036 \pm 0.003$. This is also discussed in [40]. It is, however, concluded [40] that the relevant couplings cannot be extracted from experiment in the presence of both proton and neutron components in the nuclear wave functions.

So we have to rely on the above models. The obtained results are found in Tables 1 and 2 in ref. [40]. From these, the favorite choice is

$$\begin{aligned}&C_p = 0.0663, C_n = 0.0663 \quad \text{for } \tan\beta = 1\ \text{MODEL E},\\ &C_p = 0.2712, C_n = -0.1248 \quad \text{for } \tan\beta = 10\ \text{MODEL F}.\end{aligned} \tag{16}$$

where C_p and C_n are hadronic couplings for protons and neutrons, respectively, and $\tan\beta$ is the ratio of the vacuum expectation values of the two Higgs doublets (see ref. [40]). Theoretical preference is given to the higher value of $\tan\beta$. It also yields an isovector coupling larger than the isoscalar, which is sometimes useful in obtaining the ratio of axion to photon production rates (the photon production being dominated by the isovector transition).

The effective axion-nucleon coupling can be cast in the form

$$\begin{aligned}H_{aNN} &= \frac{1}{2F_a}\left(g^0_{\mathrm{aN}} + g^3_{\mathrm{aN}}\tau_3\right)\boldsymbol{\sigma}.\mathbf{q}, g^0_{\mathrm{aN}} = \frac{1}{2}\left(C_p + C_n\right),\\ g^3_{\mathrm{aN}} &= \frac{1}{2}\left(C_p + C_n\right).\end{aligned} \tag{17}$$

Table 1: Isoscalar and isovector spin-dependent matrix elements of ^{127}I from ground ($5/2^+_{gs}$) to excited states up to to the axion energy of 5.5 MeV, which are relevant for axion photoproduction. We also include the total nuclear matrix elements $ME^2(E_x)$, including that of the spin-independent matrix elements entering in the coherent mode, which contain the factor $(1-(E_x/E_a))^3$ related to the photon energy, and the corresponding cross sections.

E_x (MeV)	Ω_0^2	Ω_1^2	$\Omega_0\Omega_1$	$ME^2(E_x)$	$\sigma \times 10^{-48}$ cm^2
0 (coherent)				4000	18714
0.0000	1.0056	0.4140	0.6452	0.8042	3.217
0.1800	0.1076	0.1243	0.1157	0.1326	0.480
0.3120	0.0194	0.0583	0.0336	0.0417	0.140
0.3150	0.0007	0.0212	-0.0038	0.0064	0.022
0.3750	0.0472	0.0314	0.0385	0.0452	0.146
0.3830	0.0023	0.0194	0.0067	0.0105	0.034
0.6490	0.0029	0.0198	-0.0076	0.0054	0.015
0.6600	0.0567	0.0481	0.0523	0.0603	0.164
0.8160	0.0241	0.0996	0.0490	0.0643	0.159
0.8340	0.0793	0.1188	0.0970	0.1120	0.274
0.8610	0.0753	0.0135	0.0319	0.0477	0.114
0.9290	0.0000	0.0001	0.0000	0.0001	0.000
0.9780	0.3952	0.3163	0.3536	0.4094	0.910
1.0440	0.0630	0.0523	0.0574	0.0663	0.141
1.1570	0.0364	0.0167	0.0247	0.0302	0.060
1.1700	0.0006	0.0006	0.0006	0.0007	0.001
1.1930	0.0026	0.0562	-0.0121	0.0166	0.032
1.2790	0.0121	0.0112	0.0117	0.0134	0.024
1.3660	0.0248	0.0093	0.0152	0.0192	0.033
1.3910	0.0029	0.0007	0.0014	0.0020	0.003
1.4780	0.0019	0.0859	0.0127	0.0365	0.057
1.6380	0.0004	0.0035	-0.0012	0.0010	0.001
1.6780	0.0005	0.0100	0.0022	0.0046	0.006
1.7610	0.0008	0.0055	0.0021	0.0031	0.004
1.9370	0.0003	0.0019	-0.0008	0.0005	0.001
1.9650	0.0006	0.0047	-0.0017	0.0013	0.001
2.1040	0.0164	0.0202	0.0182	0.0209	0.020
2.2370	0.0013	0.0097	-0.0035	0.0027	0.002
2.3140	0.0001	0.0002	0.0002	0.0002	0.000
2.4280	0.0054	0.0036	0.0044	0.0052	0.004
2.6030	0.0004	0.0002	0.0003	0.0004	0.000
2.6650	0.0030	0.0001	-0.0005	0.0011	0.001
2.7420	0.0007	0.0002	0.0004	0.0005	0.000
3.0070	0.0003	0.0005	0.0004	0.0004	0.000
3.0620	0.0003	0.0000	-0.0001	0.0001	0.000
3.1740	0.0019	0.0009	0.0013	0.0016	0.000
3.4440	0.0002	0.0001	0.0001	0.0002	0.000
3.4890	0.0002	0.0000	0.0001	0.0001	0.000
3.6020	0.0040	0.0009	0.0019	0.0027	0.000
3.9230	0.0001	0.0004	-0.0002	0.0001	0.000
3.9680	0.0000	0.0002	-0.0000	0.0001	0.000
4.0600	0.0001	0.0002	-0.0001	0.0001	0.000
4.4340	0.0004	0.0000	0.0001	0.0002	0.000
4.4560	0.0003	0.0000	0.0001	0.0001	0.000
4.5550	0.0008	0.0002	0.0004	0.0005	0.000
4.9430	0.0001	0.0000	0.0000	0.0001	0.000
4.9570	0.0000	0.0000	-0.0000	0.0000	0.000
5.0370	0.0003	0.0000	0.0001	0.0002	0.000
5.4340	0.0003	0.0000	0.0001	0.0002	0.000
5.4730	0.0000	0.0000	-0.0000	0.0000	0.000

Table 2: Isoscalar and isovector spin-dependent matrix elements of ^{23}Na from the ground ($3/2^+_{gs}$) to the various excited states entering the axion-induced photoproduction. We also include the total nuclear matrix elements $ME^2(E_x)$, including the spin-independent one appearing in the coherent mode, which contain the factor $(1-(E_x/E_a))^3$ related to the photon energy, and the relevant cross sections as well. Note that states up to the axion energy of 5.5 MeV are relevant.

E_x (MeV)	Ω_0^2	Ω_1^2	$\Omega_0\Omega_1$	$ME^2(E_x)$	$\sigma \times 10^{-48}$ cm^2
0 (coherent)				200	791
0.0000	0.4756	0.3450	0.4051	0.4721	1.889
0.4120	0.2024	0.2589	0.2289	0.2628	0.832
2.3240	0.1868	0.1286	0.1550	0.1814	0.140
2.7470	0.4689	0.3665	0.4145	0.4807	0.241
3.8930	0.0934	0.0928	0.0931	0.1069	0.011
4.3110	0.5066	0.4589	0.4821	0.5551	0.022
5.2460	0.0931	0.1184	0.1050	0.1205	0.000
5.7460	0.0474	0.0708	0.0579	0.0668	—
5.9760	0.0105	0.0046	0.0070	0.0086	—

Before proceeding further with the evaluation of the nuclear and atomic matrix elements of interest, we would like to consider the experimental situation in detecting the resulting signals using a large NaI detector, already developed and in use for rare event detection.

4. Experimental Aspects of the Axion Search by NaI

We will now briefly present some remarks on experimental aspects of the axion searches by nuclear interactions. The 5.5 MeV solar axion has been well investigated by using the Borexino detector with 278 tons of C_9H_{12} scintillation detector. Among the interactions studied are the axion-electron/photon interactions. Then, the upper limits for the product of the axion flux and the cross section are around 4.5×10^{-3} SNU, much smaller, by almost 3 orders of magnitude, than the rates for ^{8}B neutrinos without oscillation. Note the axion energy and the ^{8}B neutrino energy are similar. The limits on the axion couplings are derived as $|g^3_{aN} \times g_{aE}| \leq 5.5 \times 10^{-13}$. It is noted that the coupling $|g^3_{aN}|^2$ is studied from the axion-nuclear interaction. Experimental signals from the axion-

induced photoproduction are ultra rare 5.5 MeV γ-rays. The signal rate N_S per t y, with t being the target nuclear mass in units of ton and y being year, is given as

$$N_S = 600NA^{-1} \tag{18}$$

where N is the signal rate per 10^{27} nuclei and A is the mass number. So we get $N_S = 0.5$ and $N_S = 0.005$ for $N = 0.1$ and 0.001 in the case of $A = 127$ for iodine nuclei. We note the signal rates are just of the same order of magnitude as the rates of the neutrinoless double beta decays (DBDs), respectively, for the inverted-mass and normal-mass hierarchies (IH and NH) for typical DBD nuclei. The signal energy of 5.5. MeV is similar to that of the DBD, i.e., of around 3 MeV. Then, one may have to use multiton or even multihundred ton scale detectors as used for the IH and NH neutrino-mass DBD experiments. It is crucial for the rare-event search to reduce (BG) background counts B per t y to the level of $B \leq N_S$. Backgrounds due to radioactive impurities to be considered are the $\beta - \gamma$-rays from ^{214}Bi and ^{208}Tl. They are known to be serious in the case of DBD experiments with the signals around or below 3 MeV but are not serious in the present case of the signals above 5 MeV. Alpha particle backgrounds are separated from the γ-ray signals by a pulse-shape discrimination. The background event rate for the ^{8}B solar-neutrinos B_ν/t y is expressed [50–54] as

$$B_\nu = 0.15 \times E\Delta, \tag{19}$$

where E is the energy in units of megaelectron volt, i.e., 5.5 in the present case, and Δ is the ratio of the energy window to E. The 5.5 MeV signal rate for the realistic axion is too small to be detected beyond the background neutrinos. Thus, the search for such solar axion is not realistic at present.

In the case of the 14.4 keV axion search, the BG rate in the energy region is of the order of or larger than 1/(t y) because of all kinds of radioactive impurities in addition to the solar-neutrino BG. The background level of current low-background detectors being used for dark matter searches is of the order of 10^5/(ty). The signal to be considered is the 14.4 keV one from the axion-induced atomic electron. Then, such axions may be searched in the 5 eV region, which is interesting but not yet well investigated, by improving the background level by a few orders of magnitude. Thus, it is interesting to discuss the rate as given in Sections 9 and 10.

5. Cross Sections for Nuclear Process

Using the effective axion-nucleon coupling given by Equation (17), the nuclear matrix element (ME) is of the form

$$\mathrm{ME} = \langle \Psi_f | \mathbf{O} \bullet \mathbf{q} | \Psi_i \rangle, \quad \mathbf{O} = \sum_k \left(g^0_{\mathrm{aN}} + g^3_{\mathrm{aN}} \tau_3(k) \right) \sigma(k), \tag{20}$$

with the summation involving all nucleons. In the case of the MODEL F of Equation (16), we find $g^0_{\mathrm{aN}} = 0.073$ and $g^3_{\mathrm{aN}} = 0.197$. This can trivially be written in the proton-neutron if dictated by nuclear physics.

We will consider two processes:

(i) Nuclear excitation

$$a + A(N, Z) \longrightarrow A(N, Z)^* \tag{21}$$

followed by deexcitation emitting γ-rays

(ii) Axion photoproduction

$$a + A(N, Z) \longrightarrow A(N, Z)^* + \gamma \tag{22}$$

Note that the signals of (i) and (ii) are 5.5 MeV gammas, which are not separated. Thus, one may consider one of them, the one with the larger signal rate.

5.1. Axion-Induced Nuclear Excitation. The capture cross section associated with Figure 1(a) takes the form

$$\sigma(E_a) = \frac{1}{v} \frac{1}{2E_a} 2\pi\delta(E_a - \Delta) \mathscr{M}^2, \tag{23}$$

where Δ is the energy transferred to the nucleus. If the nuclear recoil energy is ignored, Δ corresponds to the nuclear excitation energy. $\mathscr{M}$ is the invariant amplitude, essentially the nuclear matrix element, and $1/E_a$ is the usual normalization of a scalar field. Summing over the final substates M_f and averaging over the initial substates M_i, we find

$$\sigma(E_a) = \frac{E_a}{qc^2} \frac{1}{2E_a} 2\pi\delta(E_a - \Delta) \frac{1}{(2f_a)^2} \frac{1}{3} q^2 \frac{1}{2J_i + 1} \langle J_f \| \mathbf{O} \| J_i \rangle^2, \tag{24}$$

where $\langle J_f \| \mathbf{O} \| J_i \rangle$ is the spin-reduced matrix element of the operator $\mathbf{O}$ discussed above. If the spectrum of the source is continuous given by a distribution $\rho(E_a)$, the total cross section is given by

$$\begin{aligned} \sigma(\Delta) &= \int dE_a \rho(E_a) \sigma(E_a) \\ &= \frac{\pi}{12 f_a^2} \rho(\Delta) \sqrt{\Delta^2 - m_a^2} \frac{1}{2J_i + 1} \langle J_f \| \mathbf{O} \| J_i \rangle^2, \end{aligned} \tag{25}$$

with m_a the axion mass.

In the present case, however, the spectrum resulting from the process given by Equation (1) is monochromatic and we have a resonance. So to proceed further, we assume a Breit-Wigner shape:

$$\rho(E) = \frac{1}{2\pi} \frac{\Gamma}{(E - E_a)^2 \Gamma^2}, \tag{26}$$

with a small width Γ determined by the production rate centered at the monochromatic energy, which is tiny. In fact, in the case of 14.4 keV solar axion for $m_a = 5$ eV, one finds [40] that the width $\Gamma = 10^{-24}$ eV. The situation for 5.5 MeV ^{3}He

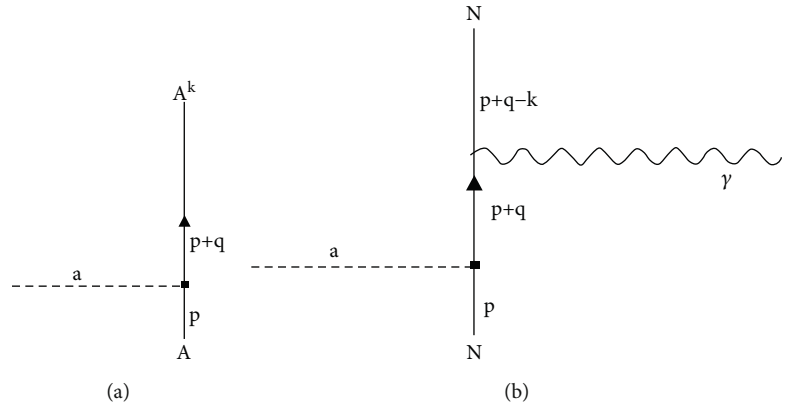

Figure 1: (a) An axion is absorbed by a nucleus leading to an excited nuclear state. (b) A Feynman diagram relevant for axion photoproduction. In both cases, in the axion vertex, we encounter the coupling given by Equation (17), while in the EM vertex in (b), we have the usual interaction involving the nuclear magnetic moment. p, q, and k are the initial nucleon, axion, and photon 4-momenta, respectively. In both cases of (a) and (b), the output signal energies are the same, 5.5 MeV.

solar axions, Equation (1), is similar. So it is reasonable to assume a flat distribution centered around E_a, that is,

$$\rho(E_a) = \begin{cases} \dfrac{1}{2\kappa\Delta}, & (1-\kappa)\Delta \le E_a \le (1-\kappa)\Delta, \quad 0 < \kappa < 1, \\ 0, & \text{otherwise.} \end{cases} \tag{27}$$

The distribution of Equation (27) is normalized the same way as that of Equation (26), that is, to unity. We thus get

$$\sigma(\Delta) = \sigma_{\mathrm{aN}} \frac{1}{2J_i+1} \left\langle J_f \| \mathbf{O} \| J_i \right\rangle^2, \qquad \sigma_{\mathrm{aN}} = \frac{\pi}{12 f_a^2} \frac{\sqrt{\Delta^2 - m_a^2}}{2\kappa\Delta}. \tag{28}$$

For axions with a mass much smaller than its energy, we find according to (11)

$$\sigma_{\mathrm{aN}} = \frac{1}{2\kappa} \times 1.00 \times 10^{-42} \mathrm{cm}^2 \left(\frac{m_a}{0.6\,\mathrm{eV}}\right)^2 \tag{29}$$

or

$$\sigma_{\mathrm{aN}} \approx \frac{1}{2\kappa} \times 6.28 \times 10^{-41} \mathrm{cm}^2 \left(\frac{m_a}{5\,\mathrm{eV}}\right)^2. \tag{30}$$

5.2. Axion Photoproduction. This process is reminiscent of the old pion photoproduction; see, e.g., [55] for a review and [56] for nuclear applications. It involves the absorption of negatively charged pion absorbed by a nucleus from a bound state in an atomic-like orbit. Since the pion is charged, the final nucleus has a different charge than the original one. There exist, of course, differences in relation to the axion having to do with its coupling, the energy, and the fact that the axion is electrically neutral, so that in this case, the final nucleus coincides with the original one. Thus, one expects the prospect an elastic coherent process as well, with a very large cross section.

The relevant elementary amplitude at the nucleon level is given in Figure 1(b).

The nonrelativistic reduction of this amplitude leads to an effective operator with the structure

$$\frac{\mu_B(N)}{f_a 2E_a} (\Omega_A + \Omega_B + \Omega_C), \tag{31}$$

with $\mu_B(N)$ the Bohr magneton for the nucleon and

$$\begin{aligned} \Omega_A &= \left(G^0_{\mathrm{aN}} + G^3_{\mathrm{aN}}\tau_3\right)(\mathbf{q} \times i\mathbf{k}) \cdot \epsilon_\lambda, \\ \Omega_B &= \left(G^0_{\mathrm{aN}} + G^3_{\mathrm{aN}}\tau_3\right)\sigma \cdot (i\mathbf{k} \times \epsilon_\lambda) E_a, \\ \Omega_C &= \left(G^0_{\mathrm{aN}} + G^3_{\mathrm{aN}}\tau_3\right)\sigma \cdot ((\epsilon_\lambda \times i\mathbf{k}) \times \mathbf{q}), \end{aligned} \tag{32}$$

where ε_λ and k are the polarization and momentum of the photon and E_a and $\mathbf{q}$ the energy and momentum of the axion. Furthermore,

$$\begin{aligned} G^0_{\mathrm{aN}} &= \frac{1}{2}\left(g_s(p)C_p + g_s(n)C_n\right), \\ G^3_{\mathrm{aN}} &= \frac{1}{2}\left(g_s(p)C_p - g_s(n)C_n\right). \end{aligned} \tag{33}$$

Using the values of Equation (16), MODEL F, we obtain

$$G^0_{\mathrm{aN}} = 0.781, \; G^3_{\mathrm{aN}} = 0.734. \tag{34}$$

We notice that in this case, we could have elastic transitions involving the spin-independent operator Ω_A. So in this case, proceeding as above, we can write

$$\mathscr{M}^2 = \frac{\mu_B^2(N)}{f_a^2 4\mathrm{E}_a^2} k^2 \mathrm{E}_a^2 \left(\mathrm{ME}^2_{el} + \mathrm{ME}^2_{i \longrightarrow f}\right), \tag{35}$$

with

$$\mathrm{ME}_{el}^2 = \left\{ \left(G_{\mathrm{aN}}^0 A + G_{\mathrm{aN}}^3 (Z-N)\right)^2 \frac{q^2}{E_a^2} \left(1 - \left(\hat{k}\cdot\hat{q}\right)^2\right) + \frac{1}{3}\frac{1}{2J_i+a} \left\langle J_i \right\| \left(G_{\mathrm{aN}}^0 + G_{\mathrm{aN}}^3 \tau_3\right)\sigma \left\| J_i \right\rangle^2 \left(1 + \frac{q^2}{E_a^2}\right) \right\}, \tag{36}$$

where k is the photon energy, which in this case is equal to the axion energy. $\mathbf{q}$ is the axion momentum, and $q^2 = E_a^2 - m_a^2 \approx E_a^2$ since the axion mass is very small. The first term in the last expression is reminiscent of the coherent contribution of all nucleons in the more familiar case of the spin-independent contribution in the WIMP-nucleus scattering (WIMP stands for weakly interacting massive particle). In deriving this expression, we have summed over all polarizations and final magnetic substates and sum over the initial m-substates. The last sum includes the contribution of both Ω_B and Ω_C, which contribute only if $J_i \neq 0$. When averaged over the photon momentum directions, the contribution of the first term is reduced by 2/3.

For transitions to excited states, we simply write

$$\mathrm{ME}_{i\longrightarrow f}^2 = \left\{ \frac{1}{3}\frac{1}{2J_i+1} \left\langle J_f \right\| \left(g_{\mathrm{aN}}^0 + g_{\mathrm{aN}}^3 \tau_3\right)\sigma \left\| J_i \right\rangle^2 \left(1 + \frac{q^2}{E_a^2}\right) \right\}. \tag{37}$$

The differential cross section, neglecting the energy of the recoiling nucleus, becomes

$$\begin{aligned} d\sigma(E_a) &= \frac{1}{v}\frac{1}{2k}\frac{1}{2E_a} 2\pi\delta(E_a - \Delta - k)\frac{1}{(2\pi)^3} \\ &\quad \cdot d^3K \mathscr{M}^2, \quad \Delta \text{ being the excitation energy} \Rightarrow \\ d\sigma(E_a) &= \frac{E_a}{qc^2}\frac{1}{2k}\frac{1}{2E_a}\frac{1}{(2\pi)^3}\frac{\mu_B^2(N)}{f_a^2 4E_a^2} k^2 E_a^2 \left(\mathrm{ME}_{el}^2 + \sum_f \mathrm{ME}_{i\longrightarrow f}^2\right) \\ &\quad \cdot 2\pi\delta(E_a - \Delta - k) 4\pi k^2 dk \\ &= \frac{E_a}{qc^2}\frac{1}{4\pi}\frac{\mu_B^2(N)}{f_a^2 4E_a^2} \left(\mathrm{ME}_{el}^2 + \sum_f \mathrm{ME}_{i\longrightarrow f}^2\right) kE_a\delta \\ &\quad \cdot (E_a - \Delta - k) k^2 dk \Rightarrow \\ \sigma(E_a) &= \frac{E_a}{qc^2}\frac{1}{4\pi}\frac{\mu_B^2(N)}{f_a^2 4E_a^2} \left(\mathrm{ME}_{el}^2 + \sum_f \mathrm{ME}_{i\longrightarrow f}^2\right) E_a (E_a - \Delta)^3. \end{aligned} \tag{38}$$

$E_a - \Delta$ is, of course, equal to the photon energy. The cross section can also be expressed in terms of the axion mass:

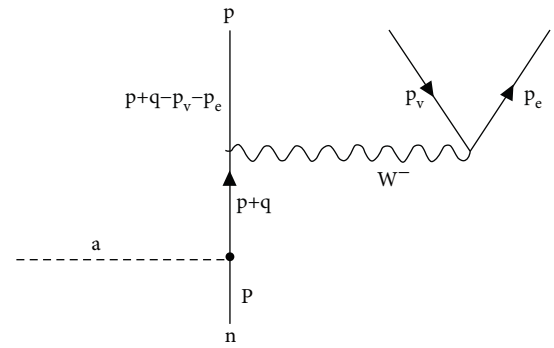

Figure 2: A Feynman diagram relevant for axion-induced beta decay.

$$\begin{aligned} \sigma(E_a) &= \sigma_0(a\gamma)\left(\mathrm{ME}_{el}^2 + \sum_f \mathrm{ME}_{i\longrightarrow f}^2\right)\left(1 - \frac{\Delta}{E_a}\right)^3, \\ \sigma_0(a\gamma) &= \frac{E_a}{qc^2}\frac{1}{4\pi}\frac{E_a^2\mu_B^2(N)}{4}\frac{1}{f_a^2}. \end{aligned} \tag{39}$$

Thus, the scale of the cross section for axion photoproduction for $f_a = 10^7$ GeV, which corresponds to $m_a = 0.6$ eV, is

$$\sigma_{a\gamma} \approx 6\times 10^{-50}\ \mathrm{cm}^2 \left(\frac{E_a}{5.5\ \mathrm{MeV}}\right)^2 \left(\frac{m_a}{0.6\ \mathrm{eV}}\right)^2 \tag{40}$$

or

$$\sigma_{a\gamma} \approx 4\times 10^{-48}\ \mathrm{cm}^2 \left(\frac{E_a}{5.5\ \mathrm{MeV}}\right)^2 \left(\frac{m_a}{5\ \mathrm{eV}}\right)^2. \tag{41}$$

This seems suppressed compared, e.g., to the axion-nucleus cross section discussed above. This is not surprising, since the axion energy of 5.5 MeV is much smaller than the nucleon mass $E_a^2\mu_B^2(N) \ll 1$. This can be overcome by the fact that many final states below E_a can contribute. Furthermore, the elastic term contains a large coherent contribution, which is proportional to A^2. We should also keep in mind that in this case, the cross section includes the radiative part as well.

5.3. Weak Process Induced by Axion Absorption. This can occur in a process given by the Feynman diagram shown in Figure 2.

Proceeding as in the previous subsection, we find the following possibilities:

$$\begin{aligned} \Omega = \frac{G_F}{\sqrt{2}}\frac{1}{f_a 2E_a} C_n E_a \Big(&((N\tau_+ N) j_0 + (N\tau_+ \sigma N)\cdot j) \\ &- (N\tau_+ N) j \cdot \frac{q}{E_a} - (N\tau_+ \sigma N)\cdot \frac{(-iq\times j)}{E_a} \Big), \end{aligned} \tag{42}$$

where C_n is the appropriate axion-neutron coupling appropriate for negaton decay.

$$j_\mu = \bar{e}\gamma_\mu(1-\gamma_5)\nu_e \tag{43}$$

is the usual weak leptonic current. The first two terms are exactly the Fermi and the GT matrix elements encountered in the allowed beta decay. The other two contribute similarly, since, for a light axion, $q^2/E_a^2 \approx 1$. So one encounters the contribution $2(ME_F^2 + ME_{GT}^2)$.

The differential cross section takes the form

$$d\sigma_{a\beta} = \frac{1}{\upsilon}\frac{1}{2E_a}\left(\frac{G_F}{\sqrt{2}}\frac{1}{f_a}C_n\right)^2 2\left(\mathrm{ME}_F^2 + \mathrm{ME}_{GT}^2\right)m^2 \cdot (p_e, p_\nu)2\pi\delta(E_a - \Delta - E_e - E_\nu)\frac{d^3p_e}{(2\pi)^3}\frac{d^3p_\nu}{(2\pi)^3}, \tag{44}$$

where Δ is the nuclear energy difference involved and $m^2(p_e, p_\nu)$ the standard leptonic matrix element. The total cross section can be cast in the form

$$\sigma_{a\beta} = \sigma_{0a\beta}\left(\mathrm{ME}_F^2 + \mathrm{ME}_{GT}^2\right)\frac{1}{m_e^5}\int p_e^2 dp_e p_\nu^2 dp_\nu m^2 \cdot (p_e, p_\nu)2\pi\delta(E_a - \Delta - E_e - E_\nu), \tag{45}$$

with

$$\sigma_{0a\beta} = \frac{1}{2}\frac{1}{(2\pi)^3}\left(G_F m_e^2\right)^2\frac{m_e}{E_a}\frac{C_n^2}{f_a^2}. \tag{46}$$

Thus, for $f_a = 10^7$ GeV, we find

$$\sigma_{0a\beta} = 1.1\times 10^{-64}\,\mathrm{cm}^2(E_a/5.5\,\mathrm{MeV})^{-1}. \tag{47}$$

Since this corresponds to $m_a = 0.6$ eV, we find

$$\sigma_{0a\beta} = 1.1\times 10^{-64}\,\mathrm{cm}^2(E_a/5.5\,\mathrm{MeV})^{-1}(m_a/0.6\,\mathrm{eV})^2 \tag{48}$$

or

$$\sigma_{0a\beta} = 7.6\times 10^{-63}\,\mathrm{cm}^2(E_a/5.5\,\mathrm{MeV})^{-1}\left(\frac{m_a}{5\,eV}\right)^2. \tag{49}$$

This is much smaller than the $\sigma_{0\gamma}$ discussed above, which is not surprising due to the fact that we now deal with a weak process. The scale of this cross section has perhaps been underestimated, scaling it with m_e rather than the energy available in the decay. This, however, is not lost, since it will show up in the integral involved in Equation (45).

In any case, it will be of interest to compare this process with the standard beta decay. Leaving aside the nuclear matrix elements, we find

$$\frac{R0_{a\beta}}{R0_\beta} = \frac{N_A\sigma_{0a\beta}\Phi(E_a)}{(1/2\pi^3)(G_F m_e^2)^2 m_e} \approx \frac{10^{27}\times 7.6\times 10^{-63}\times 1.3\times 10^9\,\mathrm{s}^{-1}}{0.016\times 9.62\times 10^{-24}7.8\times 10^{20}} = 8.3\times 10^{-23}. \tag{50}$$

Experimentally, the 5.5 MeV state, if excited, decays immediately by gamma emission with 10^{-15} sec, and thus, the weak decays are not considered experimentally as in many other cases.

Let us hope that a target with $N_A \gg 10^{27}$ is possible (in high-energy experiment searching, e.g., for proton decay, about $10^{32} - 10^{33}$ nuclei have been accumulated, but in this case, the decay products are characterized by high energy, so their detection becomes easier and, in addition, the radioactivity background is absent). If this optimistic scenario holds, the axion-induced weak process offers many advantages:

(i) Many stable nuclei might become unstable. Provided that transitions $A(N,Z)(0^+) \longrightarrow A(N-1, Z+1)(1^+)$ become energetically available with an axion energy of 5.5 MeV, one may think that the targets involved in double beta decay [57] may undergo axion-induced weak transitions. The relevant rates, however, are quite slow since the two neutrino double beta decays are faster, and, in fact, it has been observed in many systems. Better yet, such transitions involving odd nuclei with many final states, some of which may be populated even via the Fermi transition, become available

(ii) In the case of all ordinary allowed beta decay transitions, the end point energy will be shifted by 5.5 MeV in the presence of axions

(iii) Axion-induced electron capture will exhibit a spectacular feature, which is the population of an excited state in the final nucleus, not seen before, i.e., a 5.5 MeV above the highest one hitherto observed, if such a state with a similar structure exists. This can be a state not populated before, which will lead to a deexcitation γ-ray of higher energy than hitherto observed in the usual electron capture. The states already seen can also be populated in the exotic process. Thus, in this case,

$$\frac{R_{0a,\beta}^{E_x}}{R_{0\beta}^{E_x}} = \frac{R_{0a,\beta}}{R_{0\beta}}\left(\frac{E_a + \Delta + m_e - b - E_x}{\Delta + m_e - b - E_x}\right)^2, \tag{51}$$

Where Δ is the available nuclear energy (Q-value), b is the binding energy of the electron, and E_x is the excitation energy of the final nuclear state. If the nucleus is chosen so that $\Delta + m_e - b - E_x$ is very small for some state, preferably that with the highest excitation energy, one may get a large enhancement in the rate. This is similar to the well-known nuclear excitation by neutrinos, photons, mesons, and neutrons. The excited states decay mostly by gamma transitions,

Table 3: Experimental [62] and calculated magnetic moments in units of nuclear magneton $\mu_B(N)$. The magnetic moments are calculated using the standard g factors $g_{s,n} = -3.826$, $g_{s,p} = 5.586$, $g_{l,n} = 0$, and $g_{l,p} = 1$ in nuclear magneton units.

State	Experiment	Theory
$5/2^+_{gs}$	2.81	2.92
$3/2^+_1$	0.97	0.99
$7/2^+_1$	2.54	1.72

and the weak decay branch is well-known to be negligible (of the order of 10^{-15}). The gamma decays are nonnegligible in the double beta decay and axion experiments. The weak decays are known to be negligible in double beta decays and axion search experiments and thus are not considered there

Before concluding this section, we should mention that for axion-induced weak processes, the obtained rates are undetectable, especially if one uses the axion 5.5 MeV Borexino flux. We are not going to elaborate here on this point, but it will become apparent after the discussion of Section 8.2.

6. The Nuclear Model

For the evaluation of the cross sections of the processes discussed above, an essential input is the nuclear matrix elements for some targets of experimental interest, preferably those that have been used in connection with dark matter searches. Those are going to be obtained in the context of the large basis shell model.

6.1. The Target ^{127}I. In this work, we study the experimentally relevant ^{127}I for axion detection. The coherent contribution is expected to dominate in radiative axion capture, but this is pretty much independent of the details of the wave function. The spin-dependent (SD) contribution, however, depends on the details of the nuclear structure involved.

The construction of the nuclear wave functions needed for the evaluation of matrix elements entering in the corresponding scattering cross section is accomplished in the framework of the shell model. Specifically, the calculation includes the valence space $0g_{7/2}, 1d_{5/2}, 2s_{1/2}, 1d_{3/2}$, and $0h_{11/2}$ for protons and neutrons on top of a ^{100}Sn core. The diagonalization of the Hamiltonian was performed using the shell model code ANTOINE [58]. In order to make the calculations feasible, the neutron configurations were restricted to allow at most two-particle-two-hole excitations from the full $0g_{7/2}$ and $1d_{5/2}$ shells. The number of excitations into the orbitals $2s_{1/2}, 1d_{3/2}$, and $0h_{11/2}$ leads to a matrix dimension of 7.3×10^7. A more extended configuration space has been obtained in ref. [59]. Proton many-body configurations were not restricted due to small number of valence protons. The mass-dependent Bonn-C interaction [60] was used as the two-body interaction, while the single-particle energies (SPEs): $\varepsilon_{0g_{9/2}} = -0.3$ MeV, $\varepsilon_{1d_{5/2}} = 0.0$ MeV, $\varepsilon_{2s_{1/2}} = 1.3$ MeV, $\varepsilon_{1d_{3/2}} = 1.5$ MeV, and $\varepsilon_{0h_{11/2}} = 1.9$ MeV, are taken from ref. [61].

To test the quality of the structure calculations, we compare the energy spectrum and three known magnetic moments of relevant ^{127}I isotope. Three magnetic moments are known for ^{127}I. Experimental and calculated magnetic moments are given in Table 3 while in Figure 3, the corresponding energy spectrum is presented. Most of our theoretical levels agree with the experimental ones to about 100 keV. An extension of the valence space to include configurations that arise from excitations of one or more particles probably might improve the agreement between theory and experiment although there are experimental states that are still uncertain in spin and parity assignment. Note that the spin and parity of the low-lying experimental states at 0.295 MeV and 0.473 MeV are not known. The identification of these states will be a very useful test for our calculations.

The isoscalar spin-reduced matrix elements

$$\Omega_0 = \frac{\langle J_f \| \sigma \| J_i \rangle_{I=0}}{\sqrt{2J_i + 1}} = (\text{isoscalar}),$$
$$\Omega_1 = \frac{\langle J_f \| \sigma \| J_i \rangle_{I=1}}{\sqrt{2J_i + 1}} = (\text{isovector}) \tag{52}$$

from the ground state $J_i = (5/2^+)_{gs}$ to the ground state $J_i = (5/2^+)_{gs}$ and from the ground and to the final $J_f = 3/2^+, 5/2^+$ and $7/2^+$ states up to almost 6 MeV have been computed. They are presented in Figure 4. We also summarize the obtained results in Table 1. In this table, we also present the small nuclear matrix elements around the axion energy $E_a = 5.5$ MeV, since the scale of the cross section involved, see Equation (29), is orders of magnitude larger than the spin-induced cross section involved in radiative axion capture, Equation (40). We also include the huge matrix element involved in the coherent axion photoproduction.

6.2. The Target ^{23}Na. The valence space of ^{23}Na is the *sd* shell, which comprises the $0d_{5/2}$, $1s_{1/2}$, and $0d_{3/2}$ orbitals, with a ^{16}O core. Full calculations for this isotope have previously been performed in the work [63].

As expected from weak interactions, the spin-induced rates at low excitation energies are small compared to some canonical value (sum rule). Indeed,

$$\begin{aligned}
&\frac{1}{2J_i + 1} \sum_f \langle J_f \| \mathbf{O} \| J_i \rangle^2 \\
&= \sum_{M_i, M, q, f} (-1)^q \langle J_f M_f | \mathbf{O}_q | J_i M_i \rangle^2 \\
&= \sum_{M_i, M, q, f} (-1)^q \langle J_i M_i | \mathbf{O}_{-q} | J_f M_f \rangle \langle J_f M_f | \mathbf{O}_q | J_i M_i \rangle \\
&= \sum_q (-1)^q \langle J_i M_i | \mathbf{O}_{-q} \mathbf{O}_q | J_i M_i \rangle = \langle J_i M_i | \mathbf{O} \cdot \mathbf{O} | J_i M_i \rangle,
\end{aligned} \tag{53}$$

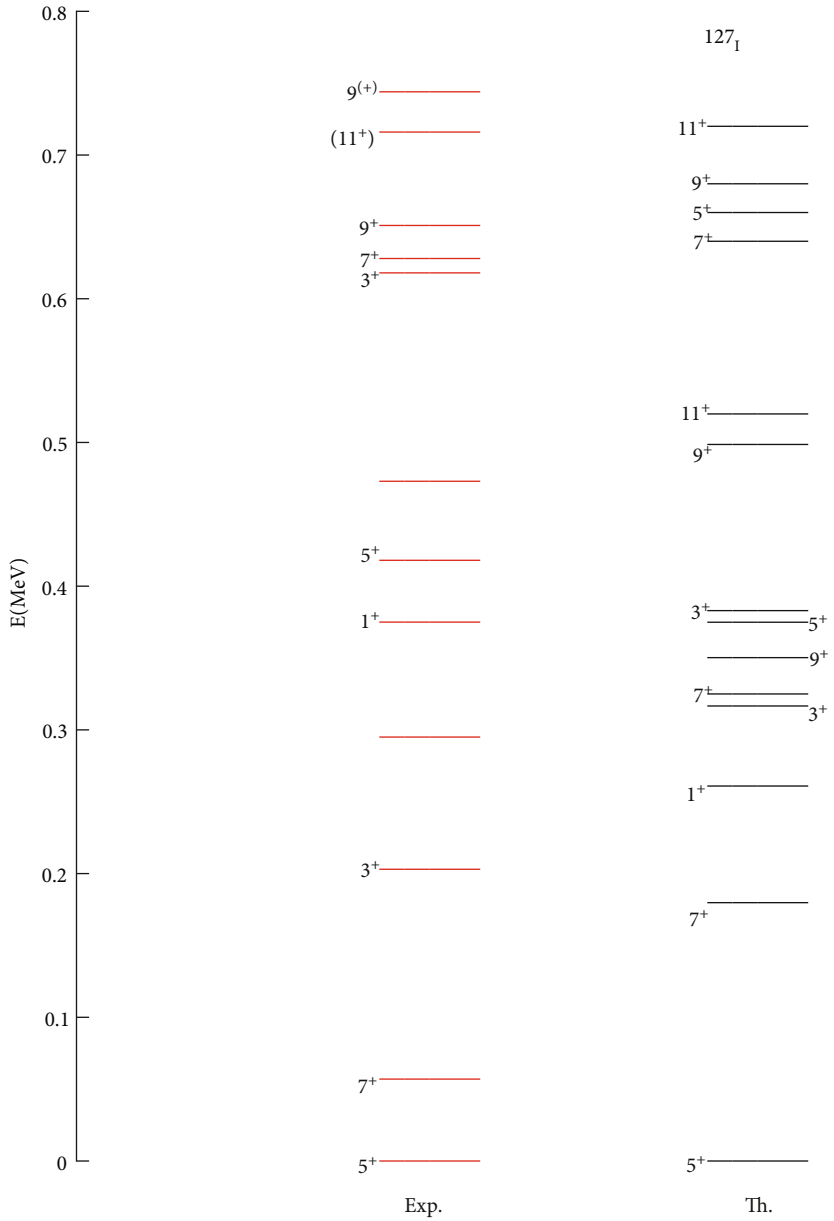

FIGURE 3: The low-lying experimental (a) [62] and theoretical (b) energy spectrum of ^{127}I. The levels in the figure are labeled by $2J$. Note that the spin and parity of the experimental states at 0.295 MeV and 0.473 MeV are not known.

with

$$\mathbf{O} = \sum_k \left(g^0_{\mathrm{aN}} + g^3_{\mathrm{aN}}\tau_3(k)\right)\sigma(k). \tag{54}$$

As a result, Equation (53) produces a one-body part which is

$$\left(\left(g^0_{\mathrm{aN}}\right)^2 + \left(g^3_{\mathrm{aN}}\right)^2\right)A + 2g^0_{\mathrm{aN}}g^3_{\mathrm{aN}}(2Z - A), \tag{55}$$

and a two-body part which is $2V$ with

$$V = \left\langle J_i M_i \left| \sum_{k\ell} \left(\left(g^0_{\mathrm{aN}} + g^3_{\mathrm{aN}}\tau_3(k)\right)\sigma(k) \cdot \left(g^0_{\mathrm{aN}} + g^3_{\mathrm{aN}}\tau_3(\ell)\right)\right)\sigma(\ell) \right| J_i M_i \right\rangle. \tag{56}$$

Since V is expected to be much smaller than that given by Equation (55), we find to a good approximation

$$S \approx \left(\left(g^0_{\mathrm{aN}}\right)^2 + \left(g^3_{\mathrm{aN}}\right)^2\right)A + 2g^0_{\mathrm{aN}}g^3_{\mathrm{aN}}(2Z - A). \tag{57}$$

We do not know the energy where this strength is located but is expected to be in the higher part of the spectrum.

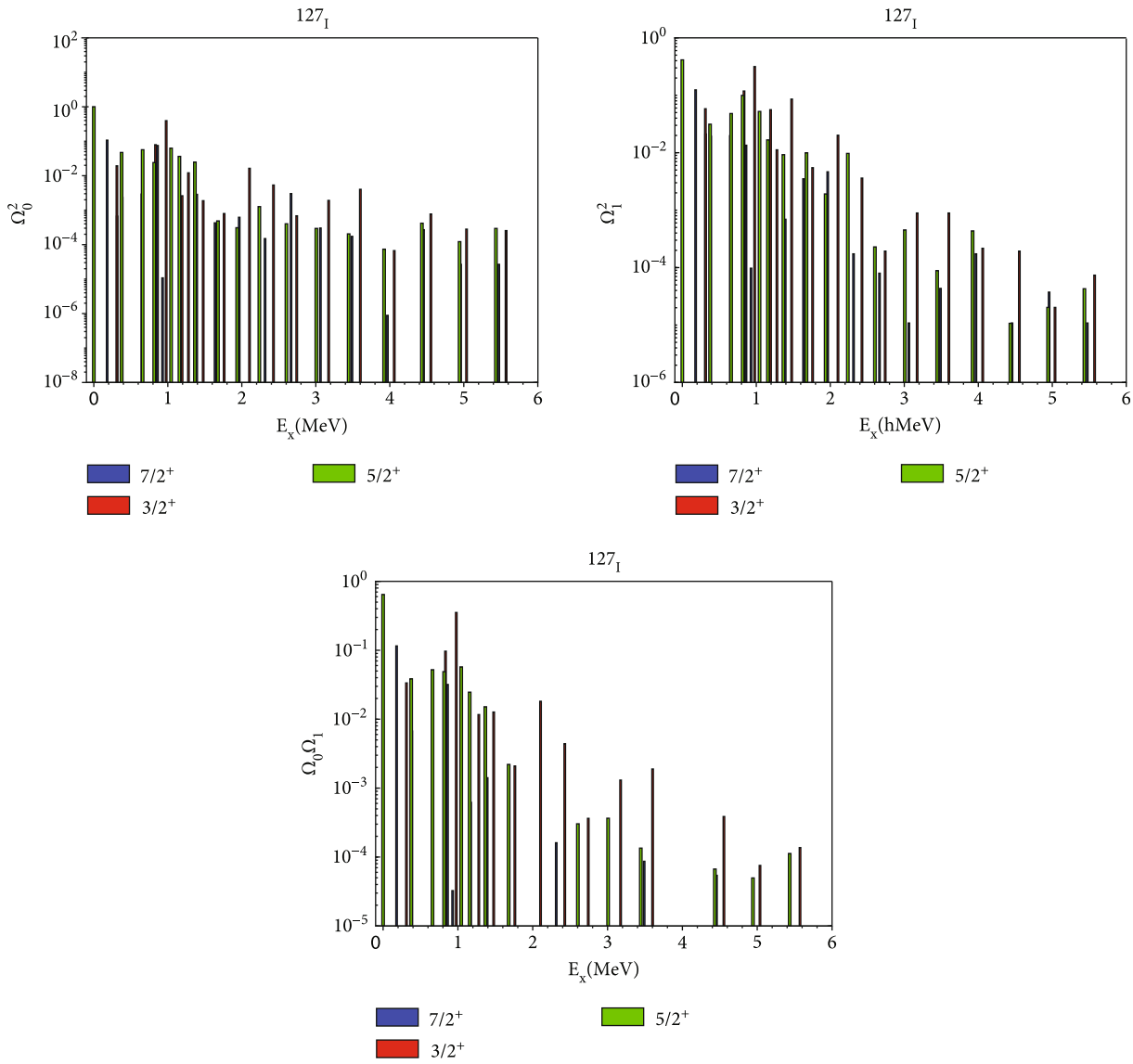

FIGURE 4: Isoscalar and isovector distribution of ^{127}I spin-reduced matrix elements from $J_i = 5/2^+_{gs}$ to J_f relevant for axion photoproduction. We should mention that the energy of the emitted photon is $E_\gamma = E_a - E_x$; i.e., the maximum photon energy corresponds to the gs to gs transition.

In the special case of interest to us using the couplings given by Equation (17) and model F of (16), we find

$$\begin{aligned} S(I) &= \left(0.083^2 + 0.192^2\right) \times 127 + 2 \times 0.083 \\ &\quad \times 0.192 \times (-11) = 5.1, \\ S(Na) &= \left(0.083^2 + 0.192^2\right) \times 23 + 2 \times 0.083 \\ &\quad \times 0.192 \times (-1) = 1.0. \end{aligned} \tag{58}$$

7. Event Rates

Noting that the oncoming beam of axions is monochromatic, the event rate is given by

$$R = \sigma \Phi(E_a) N_A, \tag{59}$$

where σ is a cross section obtained above, N_A the number of nuclei in the target, and $\Phi(E_a)$ the oncoming axion flux. We will consider two cases:

(i) The 14.4 keV Fe $*$ ^{57} flux

$$\Phi(E_a) = 0.7 \times 10^9 \left(\frac{10^7\ \text{GeV}}{f_a}\right)^2 \text{cm}^{-2}\text{s}^{-1}(14.4\ \text{keV solar axion}). \tag{60}$$

The flux has been obtained using the calculated matrix elements [40] for the ^{57}Fe$*$ deexcitation and realistic axion-nucleon coupling constants obtained in a variety of particle models.

(ii) The 5.5 MeV He-3 flux

The flux of the 5.5 MeV solar axions is obtained under the assumption that the axion production is dominated by the isovector transition and an axion mass much smaller than its energy. The standard formula for axion to photon production rate [40, 64] can be cast in the form

$$\frac{\Gamma_a}{\Gamma_\gamma} \approx 8 \times 10^{-13} \left(g_{\mathrm{aN}}^3\right)^2 \left(\frac{m_a}{5\,\mathrm{eV}}\right)^2. \tag{61}$$

From this, one can obtain the axion flux, if the photonic rate for the process of Equation (1) is known. In the Standard Solar Model (SSM), this constitutes the second stage of the pp solar fusion chain, with the first stage provided by the two reactions $p + p \longrightarrow d + e^+ + \nu_e$ and $p + p + e^- \longrightarrow d + \nu_e$. As the deuterons produced via this first stage capture protons within $\tau = 6$s, the axion flux resulting from (1) can be expressed in terms of the known pp neutrino flux [41, 43]:

$$\Phi_{\nu\mathrm{pp}} = 6.0 \times 10^{10}\,\mathrm{cm}^{-2}\mathrm{s}^{-1}(\text{solar pp neutrino flux}) \tag{62}$$

The extracted flux from the Borexino experiment [41] for the 5.5 MeV axions is given by

$$\begin{aligned}\Phi &= 2.45 \times 10^{-5}\,\mathrm{cm}^{-1}\mathrm{s}^{-1}\left(\frac{m_a}{1\,\mathrm{eV}}\right)^2 \\ &= 6.1 \times 10^{-4}\,\mathrm{cm}^{-2}\mathrm{s}^{-1}\left(\frac{m_a}{5\,\mathrm{eV}}\right)^2 \\ &= 1.86 \times 10^{4}\,\mathrm{cm}^{-2}\mathrm{y}^{-1}\left(\frac{m_a}{5\,\mathrm{eV}}\right)^2,\end{aligned} \tag{63}$$

with the last rescaled value obtained for $m_a = 5$ eV. This is many orders of magnitude smaller than that of Equation (60).

We will consider $N_A = 4 \times 10^{27}$, which is close to 1 ton of NaI in the target.

8. Some Results for Nuclear Transitions

NaI seems to be an ideal material for the detection of γ-rays. Such a target has already been employed by the DAMA experiment in dark matter searches, see, e.g.[65], and later in the DAMA/LIBRA collaboration [66].

8.1. Axion Photoproduction. Let us begin with the axion photoproduction.

(A) We will first examine the component ^{127}I of the target. We will consider two cases:

(a) Elastic scattering contributions

The first term is the coherent contribution which amounts to

$$\mathrm{ME}_{\mathrm{coh}}^2 = \frac{2}{3}\left(0.781 \times 127 + 0.734 \times (-21)\right)^2 \approx 4 \times 10^3. \tag{64}$$

The second term involves the gs⟶gs spin-induced transition obtained from Figure 5; we find

$$\begin{aligned}\mathrm{ME}_{\mathrm{gs}}^2 &= \frac{2}{3}\left(\left(G_{\mathrm{aN}}^0\Omega_0\right)^2 + \left(G_{\mathrm{aN}}^3\Omega_1\right)^2 + G_{\mathrm{aN}}^0 G_{\mathrm{aN}}^3 \Omega_0\Omega_1\right) \\ &= \frac{2}{3}\left(\left(G_{\mathrm{aN}}^0\right)^2 1.005 + \left(G_{\mathrm{aN}}^3\right)^2 0.414 + G_{\mathrm{aN}}^0 G_{\mathrm{aN}}^3 0.645\right) \\ &= 0.804.\end{aligned} \tag{65}$$

(b) Similarly for the transition to the excited state at 0.978 MeV, we obtain:

$$\begin{aligned}\mathrm{ME}_{\mathrm{gs}}^2 &= \frac{2}{3}\left(\left(G_{\mathrm{aN}}^0\Omega_0\right)^2 + \left(G_{\mathrm{aN}}^3\Omega_1\right)^2 + G_{\mathrm{aN}}^0 G_{\mathrm{aN}}^3 \Omega_0\Omega_1\right) \\ &= \frac{2}{3}\left(\left(G_{\mathrm{aN}}^0\right)^2 0.395 + \left(G_{\mathrm{aN}}^3\right)^2 0.316 + G_{\mathrm{aN}}^0 G_{\mathrm{aN}}^3 0.354\right) \\ &= 0.409\end{aligned} \tag{66}$$

Using now Equation (59) and considering only the above dominant contributions, we obtain the event rate

$$\begin{aligned}E_\gamma &= 5.5\mathrm{MeV} \leftrightarrow R_{\mathrm{coh}} \\ &= 2.9 \times 10^{-16} \times 4 \times 10 \times {}^3 \\ &\approx 1.2 \times 10^{-12}(\mathrm{t-y})^{-1}, \\ E_\gamma &= 5.5\mathrm{MeV} \leftrightarrow R\left(\frac{5^+}{2}\right)_{\mathrm{gs}} \\ &= 2.9 \times 10^{-16} \times 0.804 \\ &\approx 2.4 \times 10^{-16}(\mathrm{t-y})^{-1}, \\ E_\gamma &= 4.5\mathrm{MeV} \leftrightarrow R\left(\frac{3^+}{2}\right)_4 \\ &= 2.9 \times 10^{-16} \times 0.409 \times \left(1 - \frac{E_x}{E_a}\right)^3 \\ &= 2.9 \times 10^{-16} \times 0.409 \times 0.55 \\ &\approx 0.6 \times 10^{-16}(\mathrm{t-y})^{-1}.\end{aligned} \tag{67}$$

A state by state evaluation of the rates can be similarly obtained from the cross sections which is given in Table 1.

(B) The component ^{23}Na of the target

The obtained rates can also be obtained from the cross sections summarized in Table 2. Using these data, we find for the dominant contribution

$$R_{\mathrm{coh}} = 6 \times 10^{-14}\,(t-y)^{-1}, \tag{68}$$

expected due to the smaller A involved.

It is clear that the coherent ME is very large and dominates. We do not know of any other process that exhibits such a coherence. In pion photoproduction, see, e.g., [55] and [56], one encounters a spin-independent contribution, but this does not lead to coherence since the pion is negatively charged and stop in an atomic orbit before it is absorbed by the nucleus. Anyway, a change of the nucleus is involved. The process $(\gamma\pi^0)$ is somewhat different, but it leads to coherence. The coherent scattering of the axion is the same as the well-known coherent scattering of low-energy (large wavelengths) neutrons, photons, electrons, neutrinos, and others. They are traditionally called as elastic scattering.

In any case, we believe that the coherence is there, but, in spite of the fact that the axion photoproduction is favored by the nuclear physics, the obtained rate is not very large. This can be traced to the small axion mass which makes the relevant coupling small. The above rates were obtained with 4×10^{27} particles in the target, which amounts to 1 ton of NaI. Close to such amounts of material have in fact been used in WIMP (weakly interacting massive particles) dark matter searches [66–68].

8.2. Axion-Induced Nuclear Excitation

(A) We will begin with the target ^{127}I

In this case, we consider the excitation of the nucleus which can subsequently deexcite by γ emission. In this case, since the axion source is monochromatic, only states around E_a can be excited. The nuclear matrix elements can be obtained from those of Figure 5. Thus, we obtain

$$\begin{aligned}&\left(g_{\mathrm{aN}}^{0}\right)^{2}(0.8+0.3)\times 10^{-4}+\left(g_{\mathrm{aN}}^{3}\right)^{2}4\\&\quad\times 10^{-4}+\left(g_{\mathrm{aN}}^{0}g_{\mathrm{aN}}^{3}\right)4\times 10^{-4}=2.2\times 10^{-5}.\end{aligned}\tag{69}$$

Thus, for $\kappa = 0.1$ in Equation (30) and using Equations (59) and (63), we obtain

$$\begin{aligned}R_5 &= 1.86\times 10^{4}\times\frac{1}{0.2}\times 6.28\times 10^{-41}2.2\\&\quad\times 10^{-5}\times 4\times 10^{27}\mathrm{y}^{-1}=5\times 10^{-13}(\mathrm{t}-\mathrm{y})^{-1}.\end{aligned}\tag{70}$$

This time, the scale of the cross section is favorable, but the nuclear matrix elements are suppressed.

(B) We will continue with the target ^{23}Na

In this case, the last states of Table 2 are relevant. Proceeding as in the previous case, we obtain

$$(6.4, 1.5, 0.9, 0.07)\times 10^{-10}(\mathrm{t}-\mathrm{y})^{-1}\quad\text{in that order.}\tag{71}$$

Unlike the case of ^{127}I, the above rates for ^{23}Na appear larger, the phrase as shown in Figure 6, but still small.

In view of the very small 5.5 MeV axion flux for $m_a =$ 5 eV axions, as given by Equation (63), axion-motivated nuclear physics experiments look doomed.

As we have seen, however, the axion mass is not known. The obtained rates scale with $m_a^2 \times m_a^2$, one factor coming from the axion flux and the other of the axion-nucleus cross section. The obtained rates as a function of the axion mass for two typical cases are exhibited in Figure 7.

For a larger mass, e.g., 5 keV, the expected rates become the following:

(a) For the last four states 4.31 MeV, 5.24 MeV, 5.74 MeV, and 5.97 MeV of ^{23}Na (see Table 2) as follows:

$$R = (6.4, 1.5, 0.9, 0.07)\times 10^{2}(\mathrm{t}-\mathrm{y})^{-1},\tag{72}$$

in the case of the expressions (67), (70), and (71), respectively

The rates for ^{23}Na excitation are higher than those for ^{127}I, since it so happens that in the former case, states with larger nuclear matrix element happened to be around 5.5 MeV.

We remind the reader that only excited states with energies in a narrow window around 5.5 MeV can contribute to the process. The structure of all the other states, especially of the low-lying ones, whose energies are experimentally known and can be compared to the calculated ones, is immaterial.

(b) For the axion photoproduction rate, dominated by the coherent mode of ^{127}I, as follows:

$$R \approx R_{\mathrm{coh}} = 1.2(\mathrm{t}-\mathrm{y})^{-1}\tag{73}$$

This rate is expected to be similar to that of nuclear targets with (A, Z) close to that of ^{127}I.

As expected, this rate is quite a bit smaller than in (a), due to the fact that the axion energy of 5.5 MeV is much smaller than the nucleon mass. Note, however, that in this case, we have the extra signature of the produced photon. Since the rate is dominated by the coherent mode, the photon energy is approximately equal to the axion energy.

Note that if only the total γ-ray energy is measured, one cannot distinguish between (a) and (b).

It seems that axion masses in the keV region are not allowed by astrophysical and cosmological axion limits, see, e.g., Figure 3 of the review by Raffelt [69]. So, even though such limits are somewhat model dependent, we have to concede that axion masses in the kiloelectron volt region are not realistic and high detection rates as those mentioned above in Equations (72) and (73) are not expected.

In addition to the 5.5 MeV solar axions employed here, other solar axion sources of quite a bit lower energies can be employed in nuclear physics experiments, like the 477.6 keV ^{7}Li solar axion. A search for such axions has been carried out [70–72] by using the resonant axion absorption process. No such axions have been detected, but the data collected allowed the authors to set a limit on the ^{7}Li solar axion mass of 13.9 keV at 90% C.L. [72]. It is worth mentioning

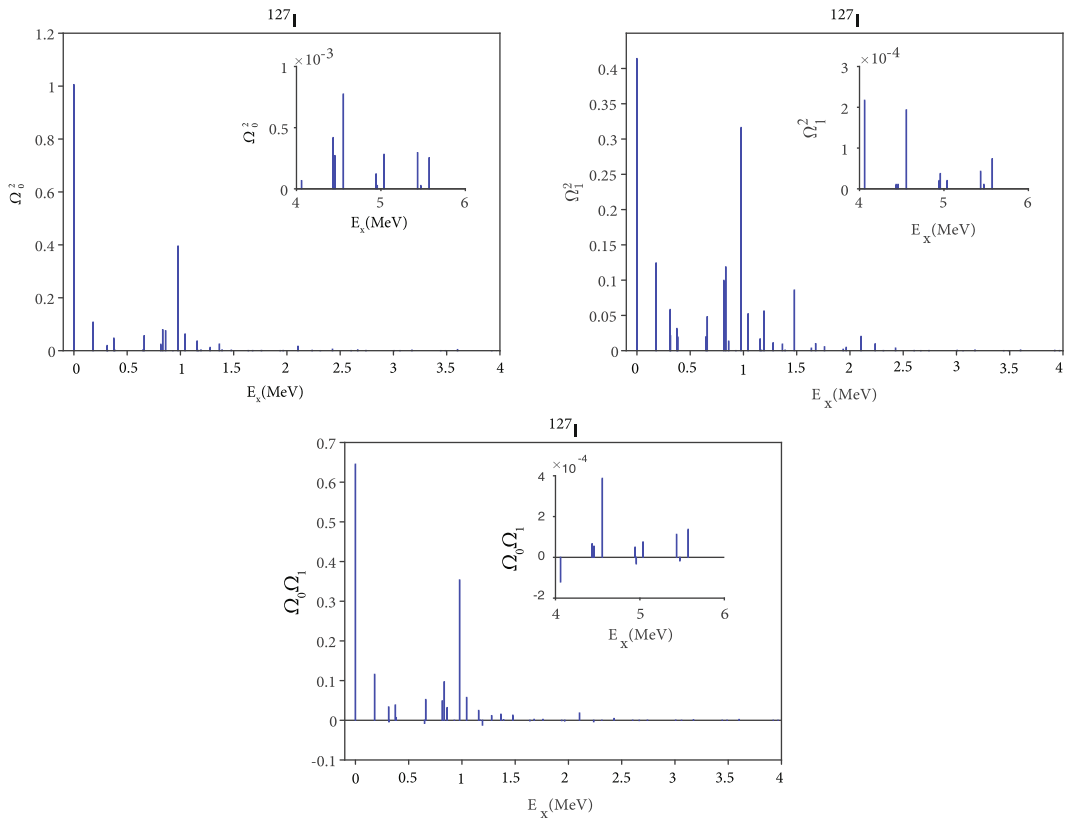

Figure 5: Isoscalar and isovector spin matrix elements up to 6 MeV relevant for axion absorption are presented. Note that in the range of 4-6 MeV, in order to make the matrix elements visible, we exhibit them in a separate small window, where the small scale is indicated.

that a LiF powder of 243 g measured during 722 h was employed, i.e., 2.0×10^{-5} (t-y). This corresponds to a detector sensitivity of about 1.5×10^{6} (t-y)$^{-1}$. It is obvious that this sensitivity needs to be improved by many orders of magnitude to reach the level of, e.g., 10^{2}(t-y)$^{-1}$ expected for 5 eV axions and relevant coupling to the electron of $g_{ae} = 024$; see Section 10.5 below. This proposal is allowed and interesting, expected to be considered in future experiments. We are not going to employ the 13.9 keV axions in this work, since the authors themselves classify their work as "preliminary results and feasibility studies."

If, instead, we use lower masses, e.g., the value of $m_a =$ 0.25keV, a model-dependent limit extracted by the CUORE experiment [34], see the discussion following Equation (82) below, we find

$$R = (6.4, 1.5, 0.9, 0.07) \times 6.25 \times 10^{-4}\,(\mathrm{t-y})^{-1}, \quad R_{\mathrm{coh}} = 7.5 \times 10^{-6}\,(\mathrm{t-y})^{-1} \tag{74}$$

quite a bit smaller than the values given by Equations (72) and (73), respectively.

For such axion masses, the detection rates in experiments involving nuclear targets may be exceedingly difficult. This, of course, can be traced back mainly to the small Borexino 5.5. MeV axion flux.

9. The Axion-Induced Processes in Atomic Targets

The presence of axion electron interaction of the form of Equation (4) gives rise to some interesting processes involving atomic targets. The most interesting are as follows:

(i) The process

$$a + A(Z)A'(Z) + \gamma, \tag{75}$$

with $A'(Z)$ the ground state or excited state of the neutral atom. This process is historically known as inverse Compton scattering or axion-induced Compton scattering

(ii) The process

$$a + A(Z_e) \longrightarrow A^*(Z_e - 1) + e^-, \tag{76}$$

where Z_e is the number of electrons in the atom. In other words, the final atom contains an electron hole. This process is historically known as axioelectric effect or axion-induced atomic excitation

9.1. The Axion Electron Coupling. Before proceeding with the evaluation of the cross section for axion-induced atomic

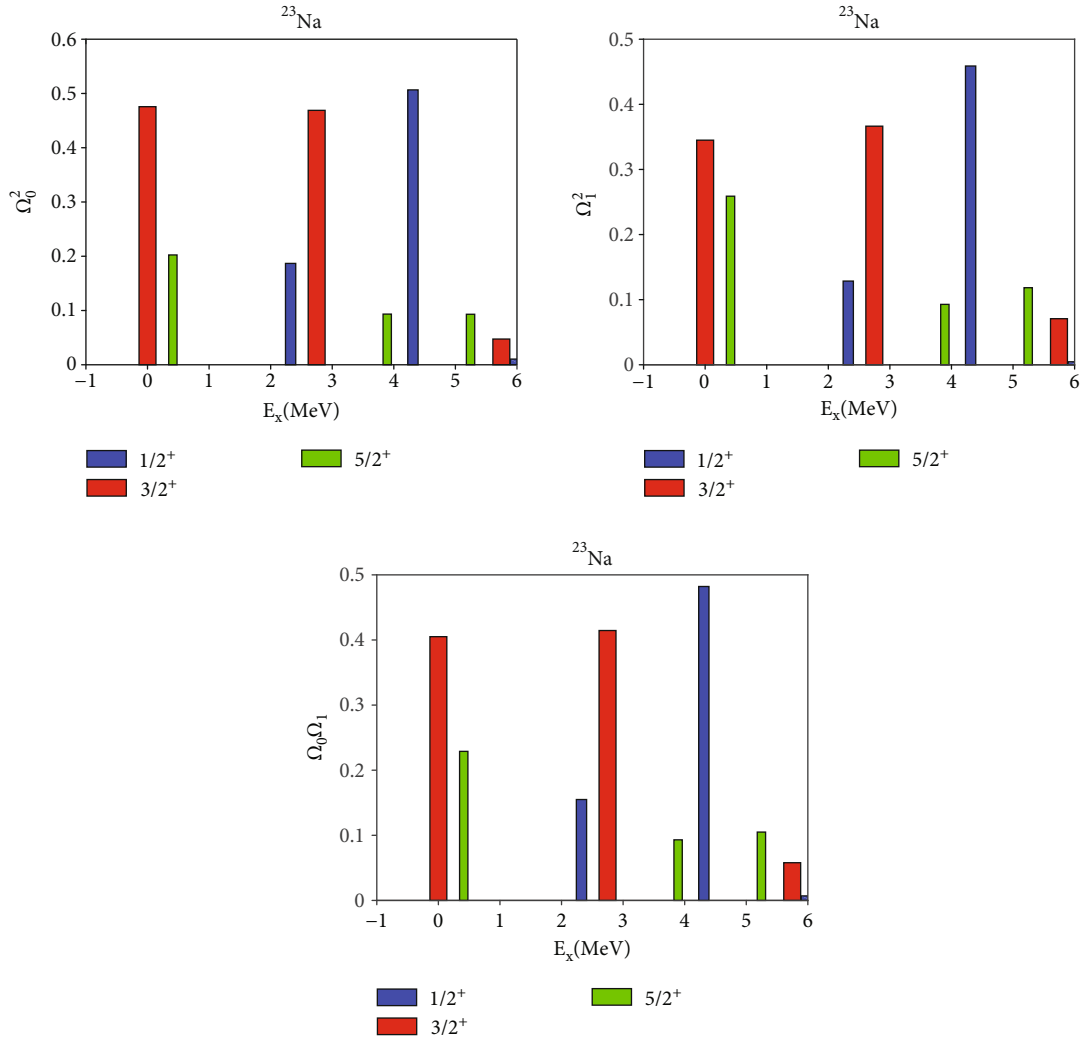

Figure 6: Isoscalar and isovector distribution of ^{23}Na spin-reduced matrix elements from $J_i = 3/2^+_{gs}$ to J_f relevant for axion photoproduction. We should mention that the energy of the emitted photon is $E_\gamma = E_a - E_x$; i.e., the maximum photon energy corresponds to the gs to gs transition.

process, we will consider the axion electron coupling (see Section 2) which can be written as

$$\mathscr{L} = G_e \sigma \cdot \mathbf{q}, G_e = \frac{g_{ae}}{2f_a}, \tag{77}$$

where g_e is a dimensionless coupling constant, which can be computed in axion models, e.g., [9]. It argued in the context of the DFSZ model [73–75] that It can be given by a relation of the form

$$g_{ae} = \frac{1}{3}\left(1 - \frac{\tan^2\beta}{1+\tan^2\beta}\right), \quad \tan\beta = \frac{v^2}{v^1}, \tag{78}$$

where v_2 and v_1 are the vacuum expectation values of the two doublets of the DFSZ model. These are not known. In such scenario, the maximum value of g_{ae} can be 1/3, but small values corresponding to the large values $\tan^2\beta$ are perhaps favored, as had been the case with supersymmetry. Be that as it may, we have decided to be conservative and adopt a relatively large value of $\tan\beta$, namely, $\tan^2\beta = 12.9$. This yields the value

$$g_{ae} = 0.024. \tag{79}$$

In any case, it will be treated as a parameter to be fixed by experiment. To make this clear, in all expressions it is going to be used, there will be a relevant accompanying factor, some power of $g_{ae}/0.024$.

On the other hand, f_a is the axion decay constant, which is related to the axion mass via Equation (11). This relation is close to that between m_a and f_a used in the analysis of the CUORE [34] and Borexino [41] experiments. Thus, for $f_a = 10^7$ GeV, we get $m_a = 0.6$ eV and selecting the value

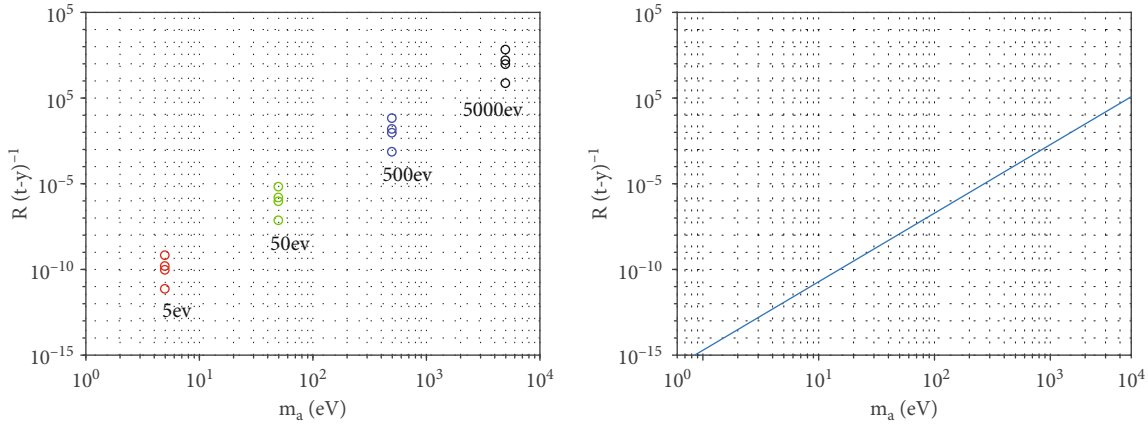

Figure 7: (a) Event rates for the last four states 4.31 MeV, 5.24 MeV, 5.74 MeV, and 5.97 MeV of ^{23}Na (see Table 2) versus different axion masses. (b) The rate for axion photoproduction on ^{127}I. As expected, this is quite a bit smaller than in (a), due to the fact that the axion energy of 5.5 MeV is much smaller than the nucleon mass. Note, however, that in this case, we have the extra signature of the produced photon. Since the rate is dominated by the coherent mode, the photon energy is approximately equal to the axion energy.

$g_{ae} = 0.024$, we find

$$G_e = 1.2 \times 10^{-12}\,\mathrm{MeV}^{-1}\left(\frac{g_{ae}}{0.024}\right)\frac{m_a}{0.6\,\mathrm{eV}} = 1.0 \times 10^{-11}\,\mathrm{MeV}^{-1}\left(\frac{g_{ae}}{0.024}\right)\frac{m_a}{5\,\mathrm{eV}}. \quad (80)$$

Thus, the scale of the cross section is

$$(\sigma_0)_e = G_e^2 = 1.0 \times 10^{-22}\,\mathrm{MeV}^{-2}\left(\frac{g_{ae}}{0.024}\right)^2\left(\frac{m_a}{5\,\mathrm{eV}}\right)^2 = 3.8 \times 10^{-44}\,\mathrm{cm}^{-2}\left(\frac{m_a}{5\,\mathrm{eV}}\right)^2\left(\frac{g_{ae}}{0.024}\right)^2. \quad (81)$$

We should mention at this point that all cross sections calculated below will remain the same, when g_{ae} and m_a are suitably scaled. For example, if g_{ae} happens to be a thousand times smaller, $g_{ae} = 2.4 \times 10^{-5}$, provided, of course, that the axion mass is three orders of magnitude larger, i.e., $m_a = 5$ keV.

The 14.4 keV axion source appears to be ideal for atomic physics experiments. The 14.4 keV source is monochromatic, produced in the sun via the ^{57}Fe∗ [40], with a flux given by Equation (60).

9.2. A Brief Summary of Limits on the Parameters m_a and f_a Extracted from Experiments. In all the calculations of the type we have performed, a crucial parameter is the axion mass m_a, which is not known. We have been using a value of $m_a = 5$ eV, but both lower and higher values are not excluded. Limits much smaller than 5 eV, of the order of megaelectron volt, typically come from astrophysics [20] (cooling of neutron stars, etc. via axion emission) or supernova (SN) explosions. Recently, bounds come from SN data [19] which vary from 10 to 50 meV in the context of KVSZ model. Such light axions are, of course, not relevant for nuclear and atomic processes considered in this work.

Higher bounds have also been given:

(a) The CUORE [34] collaboration using the 14.4 keV solar axions and measuring the axioelectric effect in the TeO_2 bolometers provides two limits on m_a:

$$m_a \le 19.2\,\mathrm{eV}, \quad m_a \le 250\,\mathrm{eV}\ \text{both at 95\%C.L.} \quad (82)$$

Strictly speaking, what the experiment yielded are limits on f_a by using the DFSZ and KSVZ model for g_{Ae}, i.e., values of $f_a \ge 3.125 \times 10^5$ GeV and $\ge 2.4 \times 10^4$ GeV, respectively. Then, they extracted the above values of m_a as implied by Equation (11).

(b) Axions of energy 14.4 keV were employed using the axion-induced excitation of ^{57}Fe, the inverse of the axion production in the sun. That is, the process $a + {}^{57}\mathrm{Fe} \longrightarrow {}^{57}\mathrm{Fe}^* \longrightarrow {}^{57}\mathrm{Fe} + \gamma$ (14.4 keV) with a sectioned Si(Li) detector arranged in a low-background facility [76]. This approach succeeded in setting a new limit on the axion couplings to nucleons, $|-1.19g_{\mathrm{aN}}^0 + g_{\mathrm{aN}}^3| \le 3.0 \times 10^{-6}$. Within the hadronic-axion model, the respective constraints on the axion mass are $m_a \le 145$ eV (at a 95% C.L.). An analysis of the CUORE sensitivity to 14.4 keV solar axion detected by inverse coherent Bragg-Primakoff conversion in single-crystal TeO_2 has been performed. The axion coupling of $g_{a\gamma\gamma}g_{\mathrm{aN}}^{\mathrm{eff}}$ to be studied by CUORE was calculated (evaluated) to be $<1.105 \times 10^{-16}$/GeV. In this analysis, an axion mass of less than 500 eV has been used [37].

Another search for solar axions [21] produced by Compton $(\gamma + e^- \longrightarrow e^- + a)$ and bremsstrahlung-like $(e^- + Z \longrightarrow e^- + Z + a)$ processes has been performed. In this case, an upper limit on the axion-electron coupling and on the axion mass, i.e., on $g_{Ae} \times m_a \le 3.1 \times 10^{-7}$ eV at (90% C.L.),

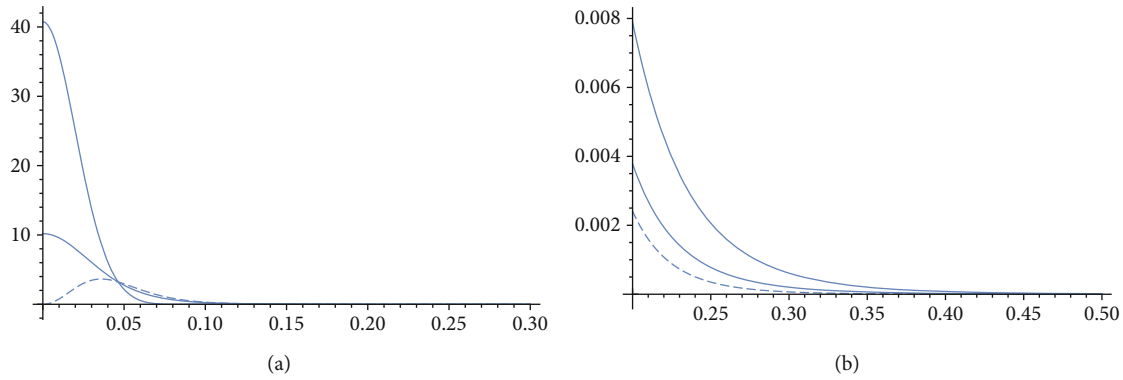

FIGURE 8: (a) We exhibit the dependence of the form factors encountered in the ionization of Na as a function of the momentum transfer, here momentum of the emitted electron p_e in units of the electron mass. (b) The same figure restricted to higher momentum transfers. The solid line corresponds to $n = 1$, the thick solid line to $n = 2, \ell = 0$, and the dashed line to $n = 2, \ell = 1$.

has been obtained. The limits on axion mass are $m_a \leq 105\,\text{eV}$ and $m_a \leq 1.3\,\text{keV}$ at the (90% C.L.) for DFSZ and KSVZ axion models, respectively.

The existence of high upper bounds on the axion mass is extremely encouraging to us in connection with this work, since they allow the possibility detectable rates involving axions in the 5 eV range, i.e., f_a around 10^6 GeV.

We stress that there exist two components in our calculation. First is the size of the oncoming axion flux, coming from the production mechanism, which can now be written as

$$\begin{aligned}\Phi(E_a) &= 0.7 \times 10^9 \left(\frac{m_a}{0.6\,\text{eV}}\right)^2 \text{cm}^{-2}\text{s}^{-1} \\ &= 2.2 \times 10^{16} \left(\frac{m_a}{0.6\,\text{eV}}\right)^2 \text{cm}^{-2}\text{y}^{-1} \\ &\quad (14.4\text{keV solar axion}).\end{aligned} \tag{83}$$

This, for convenience, can be rescaled.

$$\begin{aligned}\Phi(E_a) &= 1.5 \times 10^{18} \left(\frac{m_a}{5\,\text{eV}}\right)^2 \text{cm}^{-2}\text{y}^{-1} \\ &\quad (\text{solar for } 14.4\,\text{keV axion, rescaled}).\end{aligned} \tag{84}$$

The value for $m_a = 5\,\text{eV}$ corresponds to $f_a = 1.2 \times 10^6$ GeV.

Second is the calculated cross section, which is also proportional to m_a^2. These combined for $N_A = 4 \times 10^{27}$ particles in the target (1ton of NaI) yield a rate scaled by

$$\begin{aligned}R_0 &= 1.5 \times 10^{18} \times 4 \times 10^{27} \times 3.8 \times 10^{-44} \left(\frac{m_a}{5\text{eV}}\right)^4 \\ &= 228\ \text{events per t} - \text{y} \left(\frac{m_a}{5\text{eV}}\right)^4\end{aligned} \tag{85}$$

It seems that in the atomic experiments, one should use the value of σ_0 given by Equation (81) and the flux given by (84).

10. Some Results on Axion Electron-Induced Transitions in the Case NaI Target

In our calculations, we will consider the following processes.

10.1. Axion Photoproduction on Electrons. This process involves a special mechanism leading to the reaction given by Equation (75). In other words, in this case, the process can proceed in a manner analogous to Figure 1(b), with the obvious replacements $N \longrightarrow e$, $g_{\text{aN}}^3 \longrightarrow g_{ae}$. It involves the spin-dependent axion electron interaction as given by Equation (4) and the magnetic moment of the electron in the photon vertex. The name came from nuclear physics, the old analogous pion photoproduction process. In the atomic case, it is a special case of the axion-induced Compton scattering. It involves the gs or low-lying atomic excitations. Other possible mechanisms leading to reaction given by Equation (75), involving, e.g., the inverse Primakoff axion scattering [37, 77], will not be considered.

Let us estimate the expected cross sections, by comparing it to the hadronic process. The new feature is the Bohr magneton for the electron (as opposed to the nucleon one used before) and the axion energy dependence. Thus, for the 14.4 keV axion, we get

$$\sigma_0 = \frac{m_n^2}{m_e^2} \left(\frac{14.4\,\text{keV}}{5.5\,\text{MeV}}\right)^2 \times 6.0 \times 10^{-50} = 1.5 \times 10^{-48}\,\text{cm}^2. \tag{86}$$

See Equation (40). This, however, has been estimated with $f_a = 10^7$ GeV. Thus, in view of Equation (40), it can be written as

$$\sigma_0 = 1.5 \times 10^{-48}\,\text{cm}^2 \left(\frac{m_a}{0.6\,\text{eV}}\right)^2 = 1.1 \times 10^{-46}\,\text{cm}^2 \left(\frac{m_a}{5\,\text{eV}}\right)^2. \tag{87}$$

The dimensionless couplings will be included separately.

For the 5.5 MeV axion, we have

$$\sigma_0 = \frac{m_n^2}{m_e^2} \times 6.0 \times 10^{-50} = 2.1 \times 10^{-43}\ \mathrm{cm}^2. \tag{88}$$

The second process, of course, is not relevant, since, as we have seen, with the Borexino flux, it is undetectable. There is, of course, a coherence factor that goes with the electron axion-photoproduction, which is now proportional to Z^2. Thus, for 14.4 keV axion proceeding as in the nuclear axion photoproduction, we find

$$\sigma(E_a) = \sigma_0 G_{ae\gamma}^2 \left(\mathrm{ME}_{el}^2 + \frac{1}{3}\frac{1}{2J_i+1}\sum_f \langle J_f \| \sigma \| J_i \rangle^2 \left(1 - \frac{Ex}{E_a}\right)^3 \right), \tag{89}$$

with σ_0 given by Equation (87) and the effective axion-electron-photon coupling, analogous to those of Equation (20), is

$$\begin{aligned} G_{ae\gamma} &= g_s g_{ae} = 2 \times 0.024 = 0.048, \\ \mathrm{ME}_{el}^2 &= \left\{ \frac{2}{3} Z^2 + \frac{1}{3}\frac{1}{2J_i+1} \langle J_i \| \sigma \| J_i \rangle^2 \right\}, \end{aligned} \tag{90}$$

wherein the atomic system $E_x << E_a$.

Compare this formula with the analogous expression in nuclear transitions, Equation (35), and notice that in the present case, the spin-independent operator, see the analogous operator Ω_A in Equation (32), is just a multiple of the identity, yielding the Z^2 dependence of the square of the relevant matrix element.

The spin-reduced ME for single-particle transitions are given by

ℓ	j	j'	$\langle \ell, j' \| \sigma \| \ell, j \rangle^2$
0	$\frac{1}{2}$	$\frac{1}{2}$	6
1	$\frac{1}{2}$	$\frac{3}{2}$	$\frac{16}{3}$
1	$\frac{1}{2}$	$\frac{1}{2}$	$\frac{2}{3}$
1	$\frac{3}{2}$	$\frac{1}{2}$	$\frac{16}{3}$
1	$\frac{3}{2}$	$\frac{3}{2}$	$\frac{20}{3}$
2	$\frac{3}{2}$	$\frac{5}{2}$	$\frac{18}{5}$
2	$\frac{3}{2}$	$\frac{3}{2}$	$\frac{12}{5}$
2	$\frac{5}{2}$	$\frac{3}{2}$	$\frac{18}{5}$
2	$\frac{5}{2}$	$\frac{5}{2}$	$\frac{42}{5}$
3	$\frac{5}{2}$	$\frac{7}{2}$	$\frac{96}{5}$
3	$\frac{5}{2}$	$\frac{5}{2}$	$\frac{30}{7}$
3	$\frac{7}{2}$	$\frac{5}{2}$	$\frac{96}{7}$
3	$\frac{7}{2}$	$\frac{7}{2}$	$\frac{72}{7}$

(91)

Even for Na, the lighter component of the target, we see that the coherent contribution becomes dominant.

Thus, the obtained coherent rates, obtained with the flux given by (84), are

$$\begin{aligned} R_I &\approx 2.78 \left(\frac{g_{ae}}{0.024}\right)^2 \left(\frac{m_a}{5\mathrm{eV}}\right)^4 \text{events per(t - y)}, \\ R_{Na} &\approx \left(\frac{g_{ae}}{0.024}\right)^2 \left(\frac{m_a}{5\mathrm{eV}}\right)^4 \text{events per(t - y)} \Rightarrow R \\ &\approx 2.92 \left(\frac{m_a}{5\mathrm{eV}}\right)^4 \left(\frac{g_{ae}}{0.024}\right)^2 \text{events per(t - y)}. \end{aligned} \tag{92}$$

In this mechanism, the photons are radiated off electrons directly. As far as we know, nobody has previously considered this axion photoproduction mechanism.

The above expression does not depend on the details of the atomic structure of the target, but due to coherence only to the atomic number. Also, this process leads directly to photons with an energy equal to the axion energy E_a. Recall, however, that the scale of the cross section is proportional to E_a^2. Recalling Equation (85), we get a sort of global expression:

$$R(Z) \approx 2.50 \left(\frac{g_{ae}}{0.024}\right)^2 \left(\frac{Z}{50}\right)^2 \left(\frac{E_a}{14.4\mathrm{keV}}\right)^2 \left(\frac{m_a}{5\mathrm{eV}}\right)^4 \text{events per y} \tag{93}$$

for $N_A = 4 \times 10^{27}$.

10.2. Ejection of an Electron from an Interior Orbit. This process is described by Equation (76), but with 14.4 keV axion source, the electron hole can be in a deep bound orbit and as a result, the outgoing electron energy is $E_a + \varepsilon_b$. Such an electron can be observed directly. In addition, one may observe the X-rays and Auger electrons following the deexcitation of the final atom.

We will now proceed with estimates of the total cross section. The essential mathematical steps are given in the appendix.

For bound electrons, the cross section depends on two parameters: (a) the form factor like dependence involving the bound state wave function in momentum space $F_{n\ell} = a^3 \Phi_{n\ell}^2(a,k)$, with $\Phi_{n\ell}(a,k)$ the electron wave function in momentum space. Here, $k = q - p_e$ is the momentum transfer with q the axion momentum and p_e the momentum of the outgoing electron; (b) the phase space factor K_n, which has been evaluated with the same binding for all states in a given n. For hydrogenic bound state wave functions, we employed with $a = \alpha Z m_e / n$. The function $F_{n\ell}$ for convenience has been chosen to be dimensionless with a compensating factor a^{-3} in the phase space part to make it also dimensionless.

10.3. The Cross Section for Ionization of the Iodine Component. Bound states up to $n = 4$ were considered, with the last one being partially filled. The form factor in the case of the 14.4 keV axions is dominated by the outgoing electron

momentum $p_e = \sqrt{2m_e(E_a + \varepsilon_b)}$. The corresponding electron energies are

$$T = \{4.84,10.15,12.01\}\ \text{keV} \quad \text{for } n = 2, 3, 4, \text{ respectively} \tag{94}$$

In the case of the 5.5 MeV axions, the situation is a bit complicated and we made the simplifying assumption $k = \sqrt{q^2 + p_e^2}$. In this case, the binding energy becomes irrelevant and the electron momentum $p_e = \sqrt{E_a(E_a + 2m_e)}$.

We should mention that we summed over all states in a given full shell by introducing the $(4\ell + 2)$ factor. The form factor $F_{n\ell}$ and the kinematical factor K_n are given as follows:

$$F_{n\ell} = \begin{pmatrix} n & K(n) & F_S(n) & F_P(n) & F_D(n) & F_F(n) \\ 2 & 0.536 & 1.69994 & 14.1273 & - & - \\ 3 & 2.619 & 0.0166029 & 0.517959 & 0.854939 & - \\ 4 & 6.7547 & 0.00127243 & 0.0770985 & 0.135348 & 0.0335818 \end{pmatrix}. \tag{95}$$

The $S_{n\ell}$ factors for the cross section are given by

$$S_{n\ell} = \begin{pmatrix} n & S(S(n)) & S(P(n)) & S(D(n)) & S(F(n)) \\ 2 & 0.911049 & 7.57128 & - & - \\ 3 & 0.0434898 & 1.35675 & 2.23944 & - \\ 4 & 0.00859345 & 0.52069 & 0.914085 & 0.226797 \end{pmatrix}. \tag{96}$$

The corresponding form factor in the case of 5.5 MeV energy is given by

$$F_{n\ell} = \begin{pmatrix} n & F_S(n) & F_P(n) & F_D(n) & F_F(n) \\ 1 & 3.5376 \times 10^{-12} & 0 & 0 & 0 \\ 2 & 5.5345 \times 10^{-14} & 2.3850 \times 10^{-17} & 0 & 0 \\ 3 & 4.8600 \times 10^{-15} & 2.4813 \times 10^{-18} & 2.1373 \times 10^{-22} & 0 \\ 4 & 4.6504 \times 10^{-16} & 4.6580 \times 10^{-19} & 5.4167 \times 10^{-23} & 1.6663 \times 10^{-27} \end{pmatrix}. \tag{97}$$

The total S factor for the cross section is given by

$$S_{n\ell} = \begin{pmatrix} n & S(S(n)) & S(P(n)) & S(D(n)) & S(F(n)) \\ 1 & 7.6183 \times 10^{-8} & 0 & 0 & 0 \\ 2 & 9.53514 \times 10^{-9} & 4.1075 \times 10^{-12} & 0 & 0 \\ 3 & 2.8259 \times 10^{-9} & 1.4428 \times 10^{-12} & 1.2428 \times 10^{-16} & 0 \\ 4 & 1.1923 \times 10^{-9} & 6.4200 \times 10^{-13} & 7.4657 \times 10^{-17} & 2.2966 \times 10^{-21} \end{pmatrix}. \tag{98}$$

We see that the largest $S_{n\ell}$-factor is 7.6×10^{-8} coming for the ejection of an $0s$ electron. The form factor for this large momentum transfer leads to a great suppression of the cross section, in spite of the fact that the kinematical factor is favored, $K_n = 0.022, 0.17, 0.58, 1, 37 \times 10^6$, for 1, 2, 3, 4, respectively. In addition, the 5.5 MeV axions are not favored in atomic physics experiments due to the very small flux involved.

In the case of the 14.4 keV axions, the cross section is

$$\sigma_{n,\ell} = \sigma_0 \frac{1}{2\pi} S_{n,\ell} \tag{99}$$

(see Equation (109)), with σ_0 given by Equation (81). Thus, we get

$$\begin{aligned} \sigma_{n,\ell} = \{&0.549, 4.580, 0.0279, 0.8200, 1.353, \\ &0.005, 0.314, 0.553, 0.135\} \\ &\times 10^{-44}\ \text{cm}^2 \left(\frac{g_{ae}}{0.024}\right)^2 \left(\frac{m_a}{5\text{eV}}\right)^2 \end{aligned} \tag{100}$$

in the order of the orbitals appearing in Equation (96).

10.4. The Cross Section for Ionization of the Na Component. We do not expect a large cross section in this case because the energy of the outgoing electron is larger due to the smaller binding energy involved. Thus, one expects a lager damping on the form factors of the available $n = 1$ end $n = 2$ orbitals. In this case, we have $\varepsilon_n = (-1.646, -0.420)$ keV, respectively, for $n = 1, 2$. On the other hand, the outgoing electron energies are

$$T = \{12.75,13.99\}\text{keV} \quad \text{for } n = 1, 2 \text{ respectively.} \tag{101}$$

The suppression of the form factors at high momentum transfer, here essentially the momentum of the outgoing electron, can be seen in Figure 8 as a function of X, the momentum transfer in units of the electron mass. The actual electron momenta involved here are $X = (0.2234, 0.2340)$ for electrons ejected from $n = 1$ and $n = 2$, respectively.

In view of this, it is not surprising that, in spite of the fact the kinematical function K_n is quite large, the $S_{n\ell}$ factors are small:

$$S_{n\ell} = \begin{pmatrix} n & K(n) & S(S(n)) & S(P(n)) \\ 1 & 12.2 & 0.0424184 & - \\ 2 & 101.9 & 0.00493614 & 0.000617041 \end{pmatrix}. \tag{102}$$

Thus, using Equation (99), we find

$$\sigma_{n\ell} = \{2.567,0.298,0.036\} \times 10^{-46}\ \text{cm}^2 \left(\frac{g_{ae}}{0.024}\right)^2 \left(\frac{m_a}{5\ eV}\right)^2. \tag{103}$$

The total cross section is

$$\sigma = \sum_{n\ell} \sigma_{n\ell} = 8.36 \times 10^{-44}\ \text{cm}^2 \left(\frac{g_{ae}}{0.024}\right)^2 \left(\frac{m_a}{5\ \text{eV}}\right)^2. \tag{104}$$

This cross section scaled to $m_a = 5$ keV becomes 8.36×10^{-38} cm^2 is which between the values 10^{-36} cm^2 (DFSZ) and 10^{-41} cm^2 (KSVZ) reported by CUORE [34].

10.5. Some Results regarding the Rates for Atomic Ionization. Using now the 14.4 keV flux given by Equation (84) and $N_A = 4 \times 10^{27}$ as above, we find the following:

(i) For the iodine component

$$R_{n,\ell} = \{0.337, 2.810, 0.016, 0.503, 0.830, 0.003, 0.194, 0.340, 0.082\} \times 10^2 \text{per t} - \text{y} \left(\frac{m_a}{5\text{eV}}\right)^4 \left(\frac{g_{ae}}{0.024}\right)^2 \quad (105)$$

in the same order as in Equation (100)

(ii) For the Na component

$$R_{n,\ell} = \{1.575, 0.182, 0.022\} \text{per t} - \text{y} \left(\frac{m_a}{5\text{eV}}\right)^4 \left(\frac{g_{ae}}{0.024}\right)^2 \quad (106)$$

The obtained rates depend on the atomic wave function and in particular the form factor of the orbit involving the ejected electron. We have seen that a great suppression of the form occurs, if the axion energy is high, e.g., 5 MeV. The same thing happens in the case of a 14.4 keV axion for a small Z atom, since again, due to the small binding, the form factor is suppressed due large momentum transfer (see Figure 8). Thus, for the iodine atom, as well as others with nearby Z and the 14.4 keV energy, we have a favorable situation. One can write for the dominant contributions:

$$R_{n,\ell} = \{0.337, 2.810, 0.503, 0.829, 0.340\} \times 10^2 \text{per t} - \text{y} \left(\frac{m_a}{5\text{eV}}\right)^4 \left(\frac{g_{ae}}{0.024}\right)^2 \quad (107)$$

in the order 2S, 2P, 3P, 3D, and 4D for the orbits.

We notice the dramatic dependence of the event rate on the axion mass. Decreasing the axion mass by a factor of 5 will lead to a reduction of the rate by 3 orders of magnitude and make it unobservable; an increase by the same factor makes one wonder how come such an axion has not already been seen.

11. Concluding Remarks

In the present work, we studied various axion-induced nuclear and atomic processes, assuming an axion mass of 5 eV.

In the case of the nuclear processes, we considered the monoenergetic axion source of 5.5 MeV. The obtained nuclear cross sections were found to be reasonable, but the obtained rates were very small mainly due to the small flux on the earth of such axions, obtained with the Borexino detector [41]. So, such processes are doomed to be nondetectable for axion masses in the few electronvolt range. Had the mass of the axion been in the kiloelectron volt region, such processes would become detectable with rates as given by Figure 7 and, in particular, by Equations (72) and (73). We have seen, however, that such masses are excluded by astrophysical data. For lower axion masses in the subkeV region, e.g. the value of $m_a = 0.25$ keV, a model-dependent limit extracted by the CUORE experiment [34], the obtained total excitation and photoproduction rates in the case of NaI target become $R \approx 6 \times 10^{-3}$ and $R_{\text{coh}} \approx 1\,0^{-5}\,(t-y)^{-1}$, respectively, exceedingly difficult to detect.

In the case of atomic experiments, with inner electron binding energies in the kiloelectron volt region, we found appropriate and we used the 14.4 keV ^{57}Fe axion source. In this case, we find sizable rates, e.g.,

(i) axion-induced photoproduction. We get the rate given by Equation (93) for directly producing X-rays with energy equal to the axion energy E_a. Smaller rates are expected from the excited states with the same energy. This is independent of the details of the structure of the atom. For $m_a = 5$ eV axions ($f_a = 1.2 \times 10^6$ GeV), this leads to a rate $R \approx 2.50$ events per $(t-y)$ in the case of NaI target, assuming a coupling $g_{ae} = 0.024$

(ii) electron ejection from the atom. In this case, we find sizable rates for ejecting an electron from the relevant orbits of iodine, given by Equation (107), the maximum being 280 events per t y for $m_a = 5$ eV ($f_a = 1.2 \times 10^6$ GeV), again for $g_{ae} = 0.024$, coming from the $n = 2, \ell = 1$ orbit, and slightly smaller rates from some of the other orbits. Much smaller rates are expected for the Na component

Experiments like those discussed above have already been done by CUORE-Te [34] and others [37, 76]. As given in Equation (82), the 14.4 keV axion with the rate larger than $R = 2 \times 10^5 (t-y)^{-1} (m_a < 19$ eV DFSZ) has been excluded [34]. Then, axions in the region of $R = (10^2 - 10^4)(t-y)^{-1}$, i.e., $m_a = 5 - 10$ eV, $g_{ae} = 0.024$, are very interesting and their detection in the case of atomic excitations is quite realistic, by improving detector sensitivities by a few orders of magnitude.

If that is the case, we expect a very interesting axion signature, i.e., a signal consisting of the detection of the primarily produced electrons from each orbit as well as the detection of the X-rays or Auger electrons produced, when the created hole is filled by the deexcitation of the atom. The relevant rates depend, of course, on the assumed value of the elementary coupling g_{ae}, which is not really known.

Appendix

A. The Formalism of the Axion Electron Cross Section from Bound Orbits

The axion electron scattering cross section for relativistic axions is given by

$$d\sigma = \sigma_0 \int \mathcal{M}(k^2)^2 \frac{1}{2E_a} \frac{1 d\mathbf{p}_e^3}{(2\pi)^3} \frac{1 d\mathbf{p}_A^3}{(2\pi)^3} (2\pi) \delta(E_a + \epsilon_b - T) \cdot (2\pi)^3 \delta(\mathbf{p}_a - \mathbf{p}_A - \mathbf{p}_e), \quad (108)$$

where $M(k^2)$ is the invariant amplitude, which depends on the momentum transfer, p_e and T are the momentum and the energy of the outgoing electron and p_A of the atom, ε_b

is the binding energy of the electron in the target, and E_a is the energy of the axion, normally being introduced as a normalization of the scalar field. We have neglected the energy of the outgoing atom. Thus, integrating over p_A with the use of the momentum conserving δ function, we obtain

$$\sigma = \sigma_0 \frac{1}{2} \frac{1}{(2\pi)^2} 4\pi S = \frac{1}{2\pi} S,$$
$$S = \frac{1}{4\pi} \int \mathscr{M}\left(k^2\right)^2 \frac{1}{E_a} d\mathbf{p}_e^3 \delta(E_a + \epsilon_b - T). \tag{109}$$

Let us begin with the discussion of $M(k^2)^2$. The relevant matrix element (ME) involving the initial bound electron and the outgoing plane wave electron is given by

$$\begin{aligned} \mathrm{ME} &= \int \psi_{n\ell m}(\mathbf{r}) e^{i\mathbf{q}\cdot\mathbf{r}} \left\langle \frac{1}{2} m_s | \sigma \cdot \mathbf{q} | \frac{1}{2} m_s' \right\rangle \frac{1}{(2\pi)^{3/2}} e^{-i\mathbf{p_e}\cdot\mathbf{r}} \\ &= \sigma_{n\ell m}(\mathbf{k}) \left\langle \frac{1}{2} m_s | \sigma \cdot \mathbf{q} | \frac{1}{2} m_s' \right\rangle, \quad \mathbf{k} = \mathbf{q} - \mathbf{p_e}, \end{aligned} \tag{110}$$

where $\phi_{n\ell m}(k)$ is the initial electron bound wave function in the momentum space. The last term involves the axion electron interaction. We thus find that transition probability averaging over the initial m-substates and summing over the final ones becomes

$$\begin{aligned} &\frac{1}{(2j+1)} \sum_{m, m_\ell, m_s, m_s'} \left\langle \ell_{m\ell}, \frac{1}{2} m_s | jm \right\rangle^2 \mathrm{ME}^2 \\ &= |\sigma_{n\ell m}(\mathbf{k})|^2 \left\langle \frac{1}{2} \sum_{m_s, m_s'} \frac{1}{2} m_s | \sigma \cdot \mathbf{q} | \frac{1}{2} m_s' \right\rangle^2. \end{aligned} \tag{111}$$

The last result was obtained using the properties of the Clebcsh-Gordan coefficients. The last matrix element can easily be evaluated yielding $q^2 \approx E_a^2$ We thus find

$$S = \frac{1}{4\pi} \int |\phi_{n\ell m}(\mathbf{k})|^2 E_a d\mathbf{p}_e^3 \delta(E_a + \epsilon_b - T). \tag{112}$$

We will specialize it in the case of 14.4 keV axion. In this case, the outgoing electron is nonrelativistic $T = p_e^2/(2m_e)$; with the use of δ function, we get $p_e = \sqrt{2m_e(E_a + \varepsilon_b)}$, which is much larger than the axion momentum. So $k \approx p_e$. So after the integration over the angles, we get

$$S = \left(\phi_{n\ell m}\left(\sqrt{2m_e(E_a + \epsilon_b)}\right)\right)^2 E_a m_e \sqrt{2m_e(E_a + \epsilon_b)}. \tag{113}$$

At this point, we recall that the bound state wave function can be written as $\phi_{n\ell}(a, k)$, where k is the momentum and $a = \alpha Z m_e/n$. We prefer to write it in dimensionless form and write is as

$$\begin{aligned} &F_{n\ell}(a,k) = a^3 \phi_{n\ell}^2(a,k) \Rightarrow S = F_{n\ell} K_n, \\ &K_n = n^3 \frac{1}{(\alpha Z)^3} \frac{E_a}{(m_e)} \sqrt{2\left(\frac{E_a + \epsilon_b(n)}{m_e}\right)}. \end{aligned} \tag{114}$$

A compensating $1/a^3$ factor has been introduced in the kinematical portion of Equation (113). This way, both $F_{n\ell}$ and K_n are dimensionless.

In the case of the 5.5 MeV axion, we proceed in an analogous way. Now, the binding becomes irrelevant and the outgoing electron caries all the energy. Its momentum however is $\sqrt{E_a(E_a + 2m_e)}$, approximately the same with the axion momentum. So the angular integral is quite complicated and we made the simplifying assumption $k = \sqrt{q^2 + p_e^2}$. Now,

$$k_n = n^3 \frac{1}{\left(\alpha Z^3\right)} \left(\frac{E_a}{m_e}\right). \tag{115}$$

As expected, K_n becomes large, but the form factor $F_{n\ell}(a, k)$ at this high momentum transfer is tiny, so that the cross section becomes negligibly small.

The relevant for factors employed are given below:

$$\begin{aligned} F_{1s} &= \frac{128a^8(a-k)^2(a+k)^2}{\pi\left(a^2+k^2\right)^6}, \\ F_{0p} &= \frac{512a^{10}k^2}{3\pi\left(a^2+k^2\right)^6}, \\ F_{2s} &= \frac{32a^8\left(3a^4 - 10a^2k^2 + 3k^4\right)^2}{\pi\left(a^2+k^2\right)^8}, \\ F_{1p} &= \frac{1024a^{10}k^2(a-k)^2(a+k)^2}{\pi\left(a^2+k^2\right)^8}, \\ F_{0d} &= \frac{4096a^{12}k^4}{5\pi\left(a^2+k^2\right)^8}, \\ F_{3s} &= \frac{512a^8\left(a^6 - 7a^4k^2 + 7a^2k^4 - k^6\right)^2}{\pi\left(a^2+k^2\right)^{10}}, \\ F_{2p} &= \frac{2048a^{10}k^2\left(5a^4 - 14a^2k^2 + 5k^4\right)^2}{15\pi\left(a^2+k^2\right)^{10}}, \\ F_{1d} &= \frac{32768a^{12}k^4\left(a^2-k^2\right)^2}{5\pi\left(a^2+k^2\right)^{10}}, \\ F_{0g} &= \frac{131072a^{14}k^6}{35\pi\left(a^2+k^2\right)^{10}}. \end{aligned} \tag{116}$$

Data Availability

All data included in this manuscript are available upon request by contacting the corresponding author.

Disclosure

This manuscript version has been assigned the permanent arXiv identifier: arXiv:2104.12213v3. An earlier version of this manuscript has been presented as arXiv in http://researchgate.net/ according to the following link: https://www.researchgate.nethttps://www.researchgate.net/publication/351105232_Calculated_event_rates_for_Axion_Detection_via_Atomic_and_Nuclear_Processes/fulltext/608784218ea909241e28c9a1/Calculated-event-rates-for-Axion-Detection-via-Atomic-and-Nuclear-Processes.pdf.

Conflicts of Interest

The authors declare that they have no conflicts of interest.

Acknowledgments

J. D. V. would like to thank Georg Raffelt for his help in getting the axion mass dependence of the 14.4 keV axion solar flux.

References

[1] R. Peccei and H. Quinn, "CP conservation in the presence of pseudoparticles," *Physical Review Letters*, vol. 38, no. 25, pp. 1440–1443, 1977.

[2] S. Weinberg, "A New Light Boson?," *Physical Review Letters*, vol. 40, no. 4, pp. 223–226, 1978.

[3] F. Wilczek, "Problem of strong P and T invariance in the presence of instantons," *Physical Review Letters*, vol. 40, no. 5, pp. 279–282, 1978.

[4] J. E. Kim, "Weak-interaction singlet and strong CP invariance," *Physical Review Letters*, vol. 43, no. 2, pp. 103–107, 1979.

[5] M. A. Shifman, A. Vainshtein, and V. I. Zakharov, "Can confinement ensure natural *CP* invariance of strong interactions?," *Nuclear Physics B*, vol. 166, no. 3, pp. 493–506, 1980.

[6] M. Dine, W. Fischler, and M. Srednicki, "A simple solution to the strong CP problem with a harmless axion," *Physics Letters B*, vol. 104, no. 3, pp. 199–202, 1981.

[7] A. Zhitnisky, "Possible suppression of axion-hadron interactions," *Soviet Journal of Nuclear Physics*, vol. 31, p. 260, 1980, in Russian.

[8] L. F. Abbott and P. Sikivie, "A cosmological bound on the invisible axion," *Physics Letters B*, vol. 120, no. 1-3, pp. 133–136, 1983.

[9] M. Dine and W. Fischler, "The not-so-harmless axion," *Physics Letters B*, vol. 120, no. 1-3, pp. 137–141, 1983.

[10] J. Preskill, M. B. Wise, and F. Wilczek, "Cosmology of the invisible axion," *Physics Letters B*, vol. 120, no. 1-3, pp. 127–132, 1983.

[11] S. J. Asztalos, G. Carosi, C. Hagmann et al., "SQUID-based microwave cavity search for dark-matter axions," *Physical Review Letters*, vol. 104, no. 4, article 041301, 2010.

[12] L. Duffy, P. Sikivie, D. B. Tanner et al., "Results of a search for cold flows of dark matter axions," *Physical Review Letters*, vol. 95, no. 9, article 09134, 2005.

[13] A. Wagner, G. Rybka, M. Hotz et al., "Search for hidden sector photons with the ADMX detector," *Physical Review Letters*, vol. 105, no. 17, p. 171801, 2010.

[14] I. G. Irastorza and J. A. García, "Direct detection of dark matter axions with directional sensitivity," *Journal of Cosmology and Astroparticle Physics*, vol. 2012, no. 10, article 22, 2012.

[15] T. M. Shokair, J. Root, K. Bibber et al., "Future directions in the microwave cavity search for dark matter axions," *International Journal of Modern Physics A*, vol. 29, no. 19, article 1443004, 2014.

[16] D. J. E. Marsh, "Axion cosmology," *Physics Reports*, vol. 643, pp. 1–79, 2016.

[17] D. B. Kaplan, "Opening the axion window," *Nuclear Physics B*, vol. 260, no. 1, pp. 215–226, 1985.

[18] M. S. Turner, "Society for humanistic anthropology," *Physical Review Letters*, vol. 38, no. 6, p. 60, 1997.

[19] P. Carenza, T. Fischer, M. Giannotti, G. Guo, G. Martínez-Pinedo, and A. Mirizzi, "Improved axion emissivity from a supernova via nucleon-nucleon bremsstrahlung," *Journal of Cosmology and Astroparticle Physics*, vol. 2019, no. 10, article 16, 2019.

[20] A. V. Borisov and P. E. Sizin, "Propagation of axions in a strongly magnetized medium," *Journal of Experimental and Theoretical Physics*, vol. 83, p. 868, 1996.

[21] A. Derbin, A. Kayunov, V. Muratova, D. Semenov, and E. Unzhakov, "Constraints on the axion-electron coupling for solar axions produced by a Compton process and bremsstrahlung," *Physical Review D*, vol. 83, no. 2, article 023505, 2011.

[22] H. Primakoff, "Photo-production of neutral mesons in nuclear electric fields and the mean life of the neutral meson," *Physics Review*, vol. 81, no. 5, p. 899, 1951.

[23] K. Zioutas, S. Andriamonje, V. Arsov et al., "First results from the CERN axion solar telescope," *Physical Review Letters*, vol. 94, no. 12, article 121301, 2005.

[24] D. A. Sierra, V. de Romeri, L. J. Flores, and D. K. Papoulias, "Axionlike particles searches in reactor experiments," *Journal of High Energy Physics*, vol. 2021, no. 3, article 294, 2021.

[25] P. de Niverville, H.-S. Lee, and Y.-M. Lee, "New searches at reactor experiments based on the dark axion portal," *Physical Review D*, vol. 103, no. 7, article 075006, 2021.

[26] S. Andriamonje and E. Waxman, "Nonthermal emission from clusters of galaxies," *Journal of Cosmology and Astroparticle Physics*, vol. 2009, no. 8, article 2, 2009.

[27] M. Arik, S. Aune, K. Barth et al., "Search for solar axions by the CERN axion solar telescope withHe^3buffer gas: closing the hot dark matter gap," *Physical Review Letters*, vol. 112, no. 9, article 091302, 2014.

[28] F. Alessandria and E. V. Linder, "Constraining cosmic expansion and gravity with galaxy redshift surveys," *Journal of Cosmology and Astroparticle Physics*, vol. 2013, no. 2, article 7, 2013.

[29] T. Namba, "Results of a search for monochromatic solar axions using 57 Fe," *Physics Letters B*, vol. 645, no. 5-6, pp. 398–401, 2007.

[30] C. Arnaboldi, F. T. Avignone III, J. Beeman et al., "CUORE: a cryogenic underground observatory for rare events," *Nuclear Instruments and Methods in Physics Research Section A: Accelerators, Spectrometers, Detectors and Associated Equipment*, vol. 518, no. 3, pp. 775–798, 2004.

[31] R. Ardito, R. Ardito, C. Arnaboldi et al., "CUORE: a cryogenic underground observatory for rare events," 2005, https://arxiv.org/abs/hep-ex/0501010.

[32] D. R. Artusa, F. T. Avignone, O. Azzolini et al., "Through neutrino eyes: the search for new physics," *Advances in High Energy Physics*, vol. 2015, Article ID 879871, 13 pages, 2015.

[33] C. Alduino, K. Alfonso, E. Andreotti et al., "First results from CUORE: a search for lepton number violation via $0\nu\beta\beta$ decay of ^{130}Te," https://arxiv.org/abs/1710.07988.

[34] "Search for 14.4 keV solar axions from M1 transition of ^{57}Fe with CUORE crystals," *Journal of Cosmology and Astroparticle Physics*, vol. 2013, no. 5, article 7, 2013.

[35] N. Abgrall, I. J. Arnquist, F. T. Avignone III et al., "The Majorana Demonstrator radioassay program," *Nuclear Instruments and Methods in Physics Research Section A: Accelerators, Spectrometers, Detectors and Associated Equipment*, vol. 828, pp. 22–36, 2016.

[36] M. Agostini, M. Allardt, E. Andreotti et al., "Results on Neutrinoless Double-β Decay of Ge76 from Phase I of the GERDA Experiment," *Physical Review Letters*, vol. 111, no. 12, article 122503, 2013.

[37] D. Li, R. Creswick, F. T. Avignone III, and Y. Wang, "Sensitivity of the CUORE detector to 14.4 keV solar axions emitted by the M1 nuclear transition of ^{57}Fe," *Journal of Cosmology and Astroparticle Physics*, vol. 2016, no. 2, article 31, 2016.

[38] F. T. Avignone III, "Unconventional applications of the Ge detector and the axion," *Journal of Physics*, vol. 173, article 012015, 2009.

[39] C. Aalseth, P. S. Barbeau, N. S. Bowden et al., "Results from a search for light-mass dark matter with ap-type point contact germanium detector," *Physical Review Letters*, vol. 106, no. 13, article 131301, 2011coGeNT collaboration arXiv:10002.4703 [astro-ph.CO].

[40] F. T. Avignone III, R. J. Creswick, J. D. Vergados, P. Pirinen, P. C. Srivastava, and J. Suhonen, "Estimating the flux of the 14.4 keV solar axions," *Journal of Cosmology and Astroparticle Physics*, vol. 2018, no. 1, article 21, 2018.

[41] G. Bellini, J. Benziger, D. Bick et al., "Search for solar axions produced in thep(d,He^3)Areaction with Borexino detector," *Physical Review D*, vol. 85, no. 9, article 092003, 2012.

[42] S. Andriamonje The CAST collaboration et al., "Search for solar axion emission from 7Li and D (p,gamma) 3He nuclear decays with the CAST gamma-ray calorimeter," *Journal of Cosmology and Astroparticle Physics*, vol. 1003, p. 032, 2010.

[43] A. Bhusal, N. Houston, and T. Li, "Searching for solar axions at the Sudbury Neutrino Observatory," 2020, https://arxiv.org/abs/2004.02733.

[44] C. Patrignani, "Review of particle physics," *Chinese Physics C*, vol. 40, no. 10, article 100001, 2016.

[45] M. Gorghetto and G. Villadoro, "Topological susceptibility and QCD axion mass: QED and NNLO corrections," https://arxiv.org/abs/1812.01008.

[46] G. Bali, S. Collins, M. Göckeler et al., "Strangeness contribution to the proton spin from lattice QCD," *Physical Review Letters*, vol. 108, no. 22, article 222001, 2012.

[47] J. Li and A. W. Thomas, "Bottom quark contribution to spin-dependent dark matter detection," *Nuclear Physics B*, vol. 906, pp. 60–76, 2016.

[48] J. Ellis and E. M. Karliner, "The strange spin of the nucleon," https://arxiv.org/hep-ph/9601280.

[49] S. Pate and for the MicroBooNE Collaboration, "Progress on neutrino-proton neutral-current scattering in microboone," https://arxiv.org/abs/1701.04483.

[50] H. Ejiri, M. Ichioka, and K. Machida, "Mixed-state thermodynamics of superconductors with moderately large paramagnetic effects," *Journal of the Physical Society of Japan*, vol. 74, no. 8, pp. 2181–2184, 2005.

[51] H. Ejiri, J. Suhonen, and K. Zuber, "Neutrino–nuclear responses for astro-neutrinos, single beta decays and double beta decays," *Physics Reports*, vol. 797, pp. 1–102, 2019.

[52] H. Ejiri and K. J. Zuber, "Solar neutrino interactions with liquid scintillators used for double beta-decay experiments," *Journal of Physics G: Nuclear and Particle Physics*, vol. 43, no. 4, article 045201, 2016.

[53] H. Ejiri and S. R. Elliott, "Charged current neutrino cross section for solar neutrinos, and background to $\beta\beta(0\nu)$ experiments," *Physical Review C*, vol. 89, no. 5, article 055281, 2014.

[54] H. Ejiri and S. R. Elliott, "Solar neutrino interactions with the double-β decay nuclei ^{82}Se, ^{100}Mo, and ^{150}Nd," *Physical Review C*, vol. 95, no. 5, article 055581, 2017.

[55] M. Ericson and M. Rho, "Secretion of salivary glycoproteins," *Physics Reports*, vol. 5, p. 75, 1972.

[56] H. W. Baer, J. A. Bistirlich, N. de Botton et al., "Excitation of giant magnetic and spin-isospin dipole states in radiativeπcapture onN^{14}andB^{10}," *Physical Review C*, vol. 12, no. 3, pp. 921–937, 1975.

[57] J. D. Vergados, H. Ejiri, and F. Simkovic, "Theory of neutrinoless double-beta decay," *Reports on Progress in Physics*, vol. 75, no. 10, article 106301, 2012.

[58] E. Caurier, F. Martinez-Pinedo, A. P. Nowacki, and A. Zuker, "The shell model as a unified view of nuclear structure," *Reviews of Modern Physics*, vol. 77, no. 2, pp. 427–488, 2005.

[59] P. Klos, J. Menéndez, D. Gazit, and A. Schwenk, "Large-scale nuclear structure calculations for spin-dependent WIMP scattering with chiral effective field theory currents," *Physical Review D*, vol. 88, no. 8, article 083516, 2013.

[60] E. Caurier, F. N. Martinez-Pinedo, and A. Poves, "Influence of pairing on the nuclear matrix elements of the neutrinoless $\beta\beta$ decays," *Physical Review Letters*, vol. 100, no. 5, article 052503, 2008.

[61] M. T. Ressell and D. J. Dean, "Spin-dependent neutralino-nucleus scattering for A~127 nuclei," *Physical Review C*, vol. 56, no. 1, pp. 535–546, 1997.

[62] A. Hashizume, "Nuclear data sheets for A = 127," *Nuclear Data Sheets*, vol. 112, no. 7, pp. 1647–1831, 2011.

[63] P. C. Divari, T. S. Kosmas, J. D. Vergados, and L. D. Skouras, "Shell model calculations for light supersymmetric particle scattering off light nuclei," *Physical Review C*, vol. 61, no. 5, article 054612, 2000.

[64] R. D. Peccei, *Journal of the Korean Physical Society*, vol. 29, p. S199, 1996.

[65] R. Bernabei, P. Belli, F. Montecchia et al., "On a further search for a yearly modulation of the rate in particle Dark Matter direct search," *Physics Letters B*, vol. 450, no. 4, pp. 448–455, 1999.

[66] R. Bernabei, P. Belli, A. Bussolotti et al., "The DAMA/LIBRA apparatus," *Nuclear Instruments and Methods in Physics Research Section A: Accelerators, Spectrometers, Detectors and Associated Equipment*, vol. 592, no. 3, pp. 297–315, 2008.

[67] R. Bernabei et al., "DAMA LIBRA phase 2," *Nuclear Physics and Atomic Energy*, vol. 19, no. 4, p. 387, 2018.

[68] S. C. Kim et al., "DAMA LIBRA phase 2," *Physical Review Letters*, vol. 108, article 181381, 2012.

[69] G. G. Raffelt, "Astrophysical axion bounds," *Lecture Notes in Physics*, vol. 741, p. 51, 2008.

[70] M. Krčmar, Z. Krečak, A. Ljubičić, M. Stipčević, and D. A. Bradley, "Search for solar axions using ^{7}Li," *Physical Review D*, vol. 64, no. 11, article 115016, 2001.

[71] A. V. Derbin, A. I. Egorov, I. A. Mitropolsky, and V. N. Muratova, "Search for solar axions emitted in an M1 transition in ^{7}Li* nuclei," *JETP Letters*, vol. 81, no. 8, pp. 365–370, 2005.

[72] P. Belli, R. Bernabei, R. Cerulli et al., "^{7}Li solar axions: preliminary results and feasibility studies," *Nuclear Physics A*, vol. 806, no. 1-4, pp. 388–397, 2008.

[73] M. Srednicki, "Axion couplings to matter," *Nuclear Physics B*, vol. 260, no. 3-4, pp. 689–700, 1985.

[74] G. G. di Cortona, E. Hardy, J. P. Vega, and G. Villadoro, "The QCD axion, precisely," *Journal of High Energy Physics*, vol. 2016, no. 1, article 34, 2016.

[75] A. Ringwald and K. Saikawa, "Axion dark matter in the post-inflationary Peccei-Quinn symmetry breaking scenario," *Physical Review D*, vol. 93, no. 8, article 085031, 2016.

[76] A. V. Derbin, V. N. Muratova, D. A. Semenov, and E. V. Unzhakov, "New limit on the mass of 14.4-keV solar axions emitted in an M1 transition in 57Fe nuclei," *Physics of Atomic Nuclei*, vol. 74, no. 4, pp. 596–602, 2011.

[77] T. Abe, K. Hamaguchi, and N. Nagata, "Atomic form factors and inverse Primakoff scattering of axion," *Physics Letters B*, vol. 815, article 136174, 2021.